Spring 2011

Synthesis of Hybrid Inositol Glycan Analogues

Smita Fulzele
San Jose State University

SYNTHESIS OF HYBRID INOSITOL GLYCAN ANALOGUES

A Thesis

Presented to

The Faculty of the Department of Chemistry

San José State University

In Partial Fulfillment

of the Requirements for the Degree

Master of Science

by

Smita Fulzele

May 2011

The Designated Thesis Committee Approves the Thesis Titled

SYNTHESIS OF HYBRID INOSITOL GLYCAN ANALOGUES

by

Smita Fulzele

APPROVED FOR THE DEPARTMENT OF CHEMISTRY

SAN JOSÉ STATE UNIVERSITY

May 2011

Prof. Marc d'Alarcao	Department of Chemistry
Prof. Daryl Eggers	Department of Chemistry
Prof. David Brook	Department of Chemistry

ABSTRACT

SYNTHESIS OF HYBRID INOSITOL GLYCAN ANALOGUES

by Smita Fulzele

Inositol glycans (IGs) are small oligosaccharides exhibiting insulin-like metabolic activities in insulin-sensitive cells. The signal transduction pathways activated by IGs in these cells are still under study, but it is known that there is cross talk between the IG-signaling pathway and the insulin-signaling pathway downstream of the insulin receptor. Therefore, IGs may have potential for use in the treatment of type II diabetes mellitus. However, natural IGs are heterogeneous and difficult to isolate. Hence, synthetic IGs and their analogues have been chemically synthesized and evaluated for insulin-mimetic properties by various research groups. Unfortunately, the most biologically active IG analogues are structurally complex and difficult to synthesize.

The present work reports the progress towards designing and preparing biologically active IG analogues with short and relatively simple synthetic pathways. The strategy is to synthesize a small library of **h**ybrid **i**nositol **g**lycan **a**nalogues (HIGAs) where each HIGA consists of an inositol core covalently tethered to a variety of readily available non-carbohydrate moieties. Synthesis of one such HIGA (compound **16**) was successfully accomplished. Initial results from mass spectrometric analysis provide evidence of molecular mass of compound **16**.

ACKNOWLEDGEMENTS

I would like to start by expressing gratitude to my advisor Prof. Marc d'Alarcao, for the opportunity to be a part of his research group and for assigning a challenging but an interesting project. I appreciate his encouragement and support especially in times when completion of this project seemed far-fetched. Experience in the d'Alarcao laboratory has been immensely rewarding.

I would like to thank Dr. Daryl Eggers and Dr. David Brook for being on my committee. I appreciate the time they spent on critically evaluating my thesis.

I was delighted to start work on this project with two other musketeers, Douglas Fox and Lawrence Zieske. I appreciate all the help I received from both, during the initial stages of this project.

I would like to thank my pals from the d'Alarcao laboratory, Meenakshi Goel and Leon Castaneda, for their constant support, help, and motivation. It was great having stimulating chemical discussions with both!

I would like to thank Mike Stephens and Steven Cappelloni, technicians in the Chemistry Department, for their timely help and support.

My family is the core of who I am as a person. I thank all my family members for their timely morale boosters. My husband, Dr. Suniket Fulzele, who is my best friend, has always been there as a source of strength and encouragement. I would like to thank him for bringing out the best in me and for pushing the boundaries to become a better human being.

TABLE OF CONTENTS

LIST OF FIGURES

LIST OF SCHEMES

LIST OF ABBREVIATIONS

DIGs - Detergent Insoluble Glycolipids

DTT - Dithiothreitol

EC_{50} - Effective Concentration Producing 50% Cell Kill

Fmoc - Fluorenylmethoxy Carbonyl Chloride

GLUT - Glucose Transporter

GPIs - Glycosylphosphatidylinositols

hcDIGs - high cholesterol DIGs

HIGA - Hybrid Inositol Glycan Analogue

HPLC - High Performance Liquid Chromatography

HRMS - High Resolution Mass Spectroscopy

lcDIGs - low cholesterol DIGs

IGs - Inositiol Glycans

1, 5-IAEDAN - 5-(amino)-Naphthalene-1-Sulfonic Acid

IPGs - Inositol Phosphoglycans

IR - Insulin Receptor

IRS - Insulin Receptor Substrate

NMO - *N*-methylmorpholine *N*-oxide

NMR - Nuclear Magnetic Resonance

NRTK - Non-receptor Tyrosine Kinase

PDH - Pyruvate Dehydrogenase Phosphatase

PK (A, B,...) - Protein Kinase A, B, etc.

PLC - Phospholipase C

PLD - Phospholipase D

PI-PLC - Phosphatidylinositol-specific Phospholipase C

PL (A, B, ..) - Phospholipase A, B, etc.

PTPs - Protein Tyrosine Phosphatases

RCM - Ring-Closing Metathesis

T1DM - Type 1 Diabetes Mellitus

T2DM - Type 2 Diabetes Mellitus

TCEP - Tris-(2-carboxyethyl) Phosphine

TLC - Thin Layer Chromatogrphy

LIST OF NMR SPECTRA

CHAPTER 1

INTRODUCTION

1.1 Glycosylphosphatidylinositols

Glycosylphosphatidylinositols (GPIs) are complex glycolipids that are ubiquitous in eukaryotic cells. GPIs play an important role in anchoring proteins, polysaccharides and small oligosaccharides to cell membranes.[1] Non-protein-linked or free GPIs that exist in species such as protozoa and mammalian cells share some similarities with GPI protein anchors. Interestingly, one similarity is that both free-GPI and GPI anchors share a conserved glycan core.[2]

GPI anchors synthesized in the endoplasmic reticulum of eukaryotic cells were first characterized more than two decades ago. The phospholipase discovered in *Bacillus cereus*, which hydrolyzes GPIs and is known as phosphatidylinositol-specific phospholipase C (PI-PLC), was found to release certain proteins like alkaline phosphatases from the plasma membrane. This provided evidence of an anchoring system on the plasma membrane. Based on structural data and compositional studies on purified PI-PLC from different species like*Trypanosoma brucei*, rat Thy-1 and human and bovine erythrocyte acetylcholinesterase, the existence of GPI anchors was confirmed in 1985. In 1988, the first structure of a GPI anchor was resolved from *Trypanosoma brucei* (Figure 1).[3] Today hundreds of GPI-anchored proteins are known from human and a variety of protozoa, fungi, and other eukaryotes.

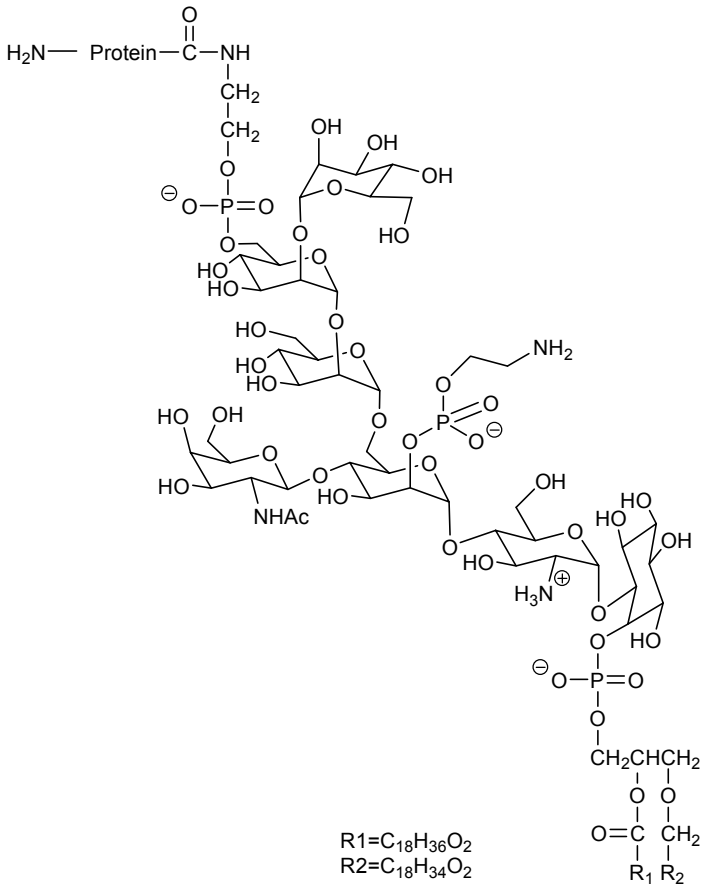

Figure 1. Structure of GPI anchor from *Trypanosoma brucei*.

1.1.1 Structure of GPI anchors

GPI anchors have a complex structure with a highly conserved core structure. The conserved core structure consists of three parts: a glycan core, a linker and a tail (Figure 2).[4] The GPI-anchored protein links to the core glycan through an ethanolamine bridge. The core glycan consists of mannose (α1-2) mannose-(α1-6) mannose (α1-4) glucosamine (α1-6)-*myo*-inositol. A

phospholipid tail extends from carbon one of *myo*-inositol and anchors to the cell membrane.

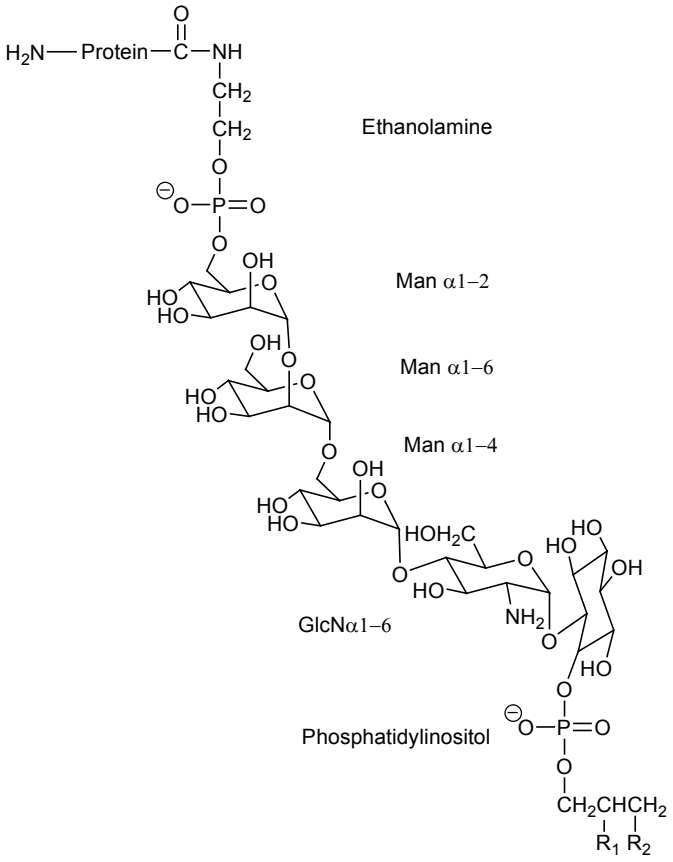

Figure 2. General structure of a GPI anchor.

The phospholipid tail and the core glycan structure have variations in structure imparting heterogeneity to the GPI anchors. Additionally, mannose residues can have side chain modifications (e.g., galactose, sialic acid).[5]

1.1.2 Role of GPIs

GPIs are suggested to be involved in numerous biological activities. However, the only confirmed biological function of the GPI anchor is to provide the protein a stable membrane-anchoring tool. Other biological functions where GPI anchors could have a putative role include lipid-raft partitioning, cellular communication, signal transduction, and apical membrane targeting.[6] GPI phospholipids are also thought to be precursors to biologically active inositol phosphoglycan (IPG) or inositol glycans (IGs). PI-PLC hydrolyzes the phosphodiester bond of phosphatidylinositol to form 1, 2-diacylglycerol and glycopeptide-bound (in GPI anchor) or glycan-bound (in free-GPI) inositol-1, 2-cyclic-phosphate. Glycosylphosphatidylinositol-specific phospholipase D (GPI-PLD) can also hydrolyze GPI anchors. The hydrolysis products of GPI-PLD are phosphatidic acid and IPG lacking a cyclic phosphate, as shown in Figure 3.[2,7] Hydrolysis of GPI phospholipids generates different types of IPGs (also known as phosphotidylinositol glycan). At least two IPGs, IPG type A and IPG type P, are known. IPG type A contains *myo*-inositol and glucosamine, and IPG type P contains α-pinitol, which is 3-O-methyl D-*chiro*-inositol and galactosamine along with additional sugar and phosphate residues. A complete structure of an IPG-P reported in literature contains a disaccharide of α–pinitol and galactosamine with Mn^{2+}. It was shown to activate pyruvate dehydrogenase phosphatase.[8] The hydrolysis products are potential insulin second messengers because they demonstrate insulin-mimetic activities; [9] this issue will be discussed in later

sections on IPGs. However, the generation of IPG from GPI glycolipids remains a topic of debate, as the exact source of IPG is yet to be determined.

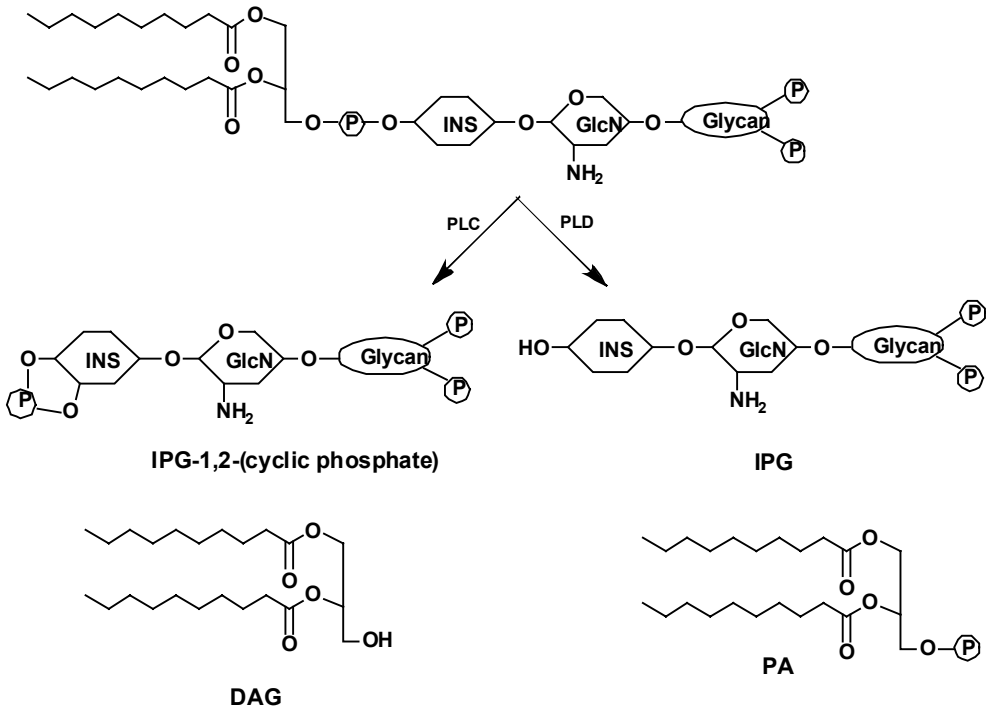

Figure 3. Mechanism of hydrolysis of GPI phospholipid by PLC and PLD. INS: *myo*-inositol; GlcN: glucosamine; PA: phosphatidic acid; DAG: diacylglycerol

1.2 Inositolphosphoglycans

IPGs were first identified in 1986 from bovine liver treated with insulin.[10] A number of in vitro studies established that IPGs exhibit insulin-mimetic properties. IPGs mimicked insulin's phosphorylation pattern in freshly isolated adipocytes.[11] Misek and Saltiel in 1992, studied the effects of an IPG generated by pronase digestion from *Trypanosoma brucei* membrane glycoprotein on rat

adipocytes and hepatocytes. It was demonstrated that IPG inhibits lipolysis, (inhibiting lipid breakdown), glucose 6-phosphatase and fructose-1, 6-diphosphatase.[12] Further, in an in vivo study, two IPGs in streptozotocin diabetic rats exhibited insulin-like action by reducing dose-dependent hyperglycemia.[13] Such studies indicated that IPGs are potential second messengers of insulin action and play a role in insulin signaling. This characteristic property of the IPG can be vital and hence exploited for the treatment of type II diabetes mellitus where insulin resistance is the cause of the disease.

1.3 Overview of diabetes mellitus

1.3.1 Glucose homeostasis

Glucose, a vital source of energy for cells, is under homeostatic control of the body which maintains glucose levels within a narrow range of 4–7 mmol/L. Glucose homeostasis relies on the balance of two hormones, insulin and glucagon. Both hormones are secreted by islet cells of the pancreas, insulin by pancreatic β-cells and glucagon by pancreatic α-cells. Insulin and glucagon are both secreted in response to blood glucose level but are opposite in action. Insulin decreases blood glucose level while glucagon increases it. Briefly, the process starts when food is consumed and broken down into fat, protein and carbohydrates. During the process of digestion, carbohydrates are further broken down into simple sugars, one of which is glucose. Glucose gets absorbed in the blood stream and is carried to cells. Sensing increased levels of glucose in the blood stream, the pancreas produces and releases insulin in the

blood stream. Insulin binds to the insulin receptor on the cells (fat or muscle cells), and facilitates glucose uptake by the cells where it is used for energy or stored in glucogen or fat. Thus, insulin decreases the blood glucose level. When the level of glucose in the blood drops below the desired level, the pancreas releases glucagon, which signals the break down of glycogen into glucose, and its release in the blood stream. In this way, glucose level is maintained between 4-7 mmol/L. However, the inability of the body to maintain the normal range of blood sugar levels can be reflective of a medical condition. High blood glucose level is referred to as hyperglycemia, and it characterizes the complex disease, diabetes mellitus.

1.3.2 Diabetes mellitus

Diabetes mellitus is a chronic endocrine disorder affecting almost 170 million people of all age groups, families and diverse societies worldwide. In the U.S. alone, 23.6 million (i.e. 7.8% of the population) have diabetes. These numbers are expected to increase to 48 million by year 2050. The cost of diabetes care accounts for over 12% of all health care costs, nearly $200 billion per year which results in a significant burden on the country's health budget.[14] Slow progression of symptoms and the complex nature of the disease makes early diagnosis difficult. Diabetes is characterized by hyperglycemia, and the two reasons for the inability of cells to take up glucose are used to describe the two types of diabetes: type 1 diabetes mellitus (T1DM) and type 2 diabetes mellitus (T2DM). T1DM is characterized by diminished or no insulin production. It was

previously known as insulin-dependent diabetes mellitus. The pancreas is not able to produce insulin because the β-cells has been destroyed. Insulin resistance and impairment of insulin secretion characterize T2DM. It was previously known as non-insulin dependent diabetes mellitus or adult-onset diabetes. T2DM is more prevalent than T1DM, accounting for 90% of the total population diagnosed with diabetes. Other less prevalent forms of diabetes include gestational diabetes (glucose intolerance during pregnancy), pre-diabetes and diabetes developed due to pancreatic disease, medications, surgery or other genetic condition.

T2DM commences as insulin resistance, which is the inability of insulin to stimulate the target cells to take up glucose. This increased glucose level is compensated by overproduction of insulin by the pancreatic β-cells. Over a period of time, β-cell function declines leading to hyperglycemia. Excessive production of glucose by breakdown of glycogen in the liver, increased insulin resistance due to obesity and decreased levels of glucagon-like peptide 1 are also factors that are associated with the disease condition.[15] Genetic, environmental and other lifestyle factors are also thought to play a role. However the exact causes of T2DM remains unknown.[16]

Insulin resistance is the major defect in the pathogenesis of T2DM and insulin resistance is linked to some flaws in the insulin signal transduction.[17] Thus, understanding the intracellular insulin signaling transduction pathway may provide insights into the origin of insulin resistance and pathogenesis of T2DM.

1.4 Overview of insulin signal transduction

The discovery of the insulin receptor in 1985 led to significant progress in understanding insulin signal transduction.

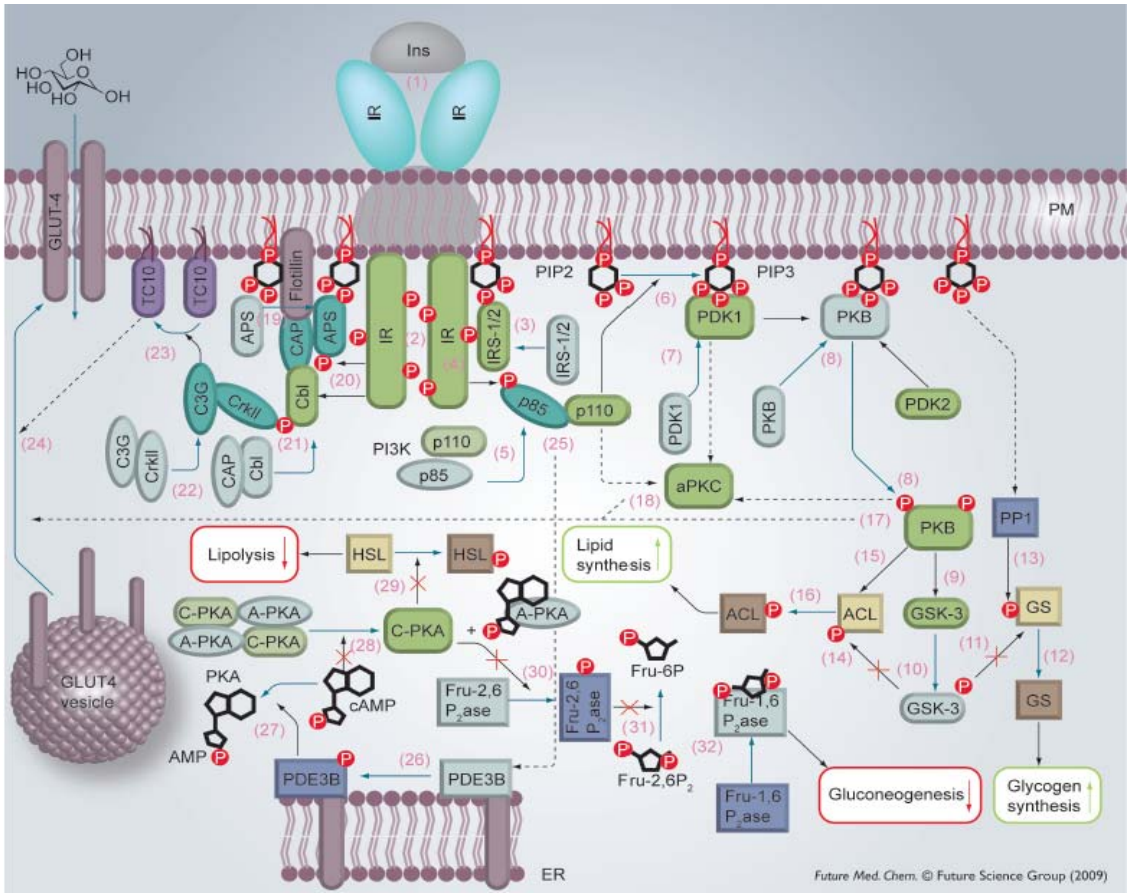

Figure 4. Schematic representation of insulin signal transduction. (Reproduced from Future Medicinal Chemistry (2009), 1(1), 95-118 with permission of Future Science Ltd).

One of the established and better-understood insulin-signaling pathways involves phosphorylation on tyrosine residues of the insulin receptor that leads to a phosphorylation cascade downstream of the insulin receptor (Figure 4).

Insulin binds on the α-subunit of the insulin receptor leading to conformational changes in the β-subunit of the insulin receptor. This conformational change activates a phosphorylation cascade, and the cytosolic subunits of the insulin receptor (IR) phosphorylate each other exhibiting increased kinase activity. This increased kinase activity increases the affinity of the cytosolic subunits towards other insulin receptor substrate (IRS). The tyrosine residues of the IRS are phosphorylated upon binding to the IR to which the regulatory domain (p85) of PI3 kinase binds. Binding of p85 leads to the generation of lipid phosphatidylinositol-3, 4, 5-triphosphate by phosphorylation of phosphatidylinositol-4, 5-diphosphate. This increases the concentration of lipid phosphatidylinositol-3, 4, 5-triphosphate and leads to a cascade of phosphorylation reactions of various proteins. The concentration of PIP3 is further controlled by two enzymes, Ship 2 and Phen.[18] Phosphoinositide-dependent kinase 1 and a second putative kinase named phosphoinositide-dependent kinase 2, binds and activates protein kinase B (PKB). Activated PKB is suggested to be a key element in insulin's metabolic action and is believed to be involved in almost all of insulin's actions like glycogen synthesis, glucose transport and protein synthesis in muscle cells and adipocytes.[19] Glycogen synthesis is initialized by phosphorylation of glycogen synthase kinase by PKB which deactivates glycogen synthase kinase but leads to activation of glycogen synthase, ultimately leading to glycogen synthesis. Deactivation of glycogen synthase kinase results in a reduced level of phophorylation of adenosine tri

phosphate citrate lyase, but phosphorylation by PKB at a different site on the adenosine triphosphate citrate lyase increases the activity of adenosine triphosphate citrate lyase. Further, adenosine triphosphate citrate lyase catalyzes conversion of citrate to acetyl co-enzyme A that is utilized in lipid synthesis. Glucose uptake is another metabolic action of insulin. There are two different pathways through which groups of glucose transporter (GLUT) proteins facilitate glucose uptake by cells, although they are yet to be characterized. One pathway involves activation of GLUT4 vesicles directly by PKB or activation through an atypical protein kinase C (PKC), while the second commences directly below the IR. Activation of IR, post insulin binding, leads to phosphorylation of Cb1 and an adaptor protein, Cb1 associated proteins, which exist as a complex. The phosphorylated complex then interacts with Crk II, which is associated with a guanine nucleotide exchange factor of the Rho-family. TC10, a member of guanosine triphosphate-binding protein family, is activated by guanine nucleotide exchange factor, and this leads to GLUT4 translocation via adaptor proteins by a mechanism that is not fully elucidated.[20] In addition to glucose storage, insulin mediates the breakdown of lipids (lipolysis) and inhibits the production of glucose in the liver (gluconeogenesis). A phosphodiesterase 3B is activated by an unknown mechanism that reduces the cyclic adenosine monophosphate levels by hydrolysis. Reduced cyclic adenosine monophosphate levels reduce protein kinase A (PKA) activity, which in turn fails to phosphorylate hormone sensitive lipase. The inactive (unphosphorylated) form of hormone

sensitive lipase thus reduces lipolysis. Inactive PKA also fails to phosphorylate fructose 2, 6-bisphosphatase and prevents conversion of fructose 2, 6-bisphosphate to fructose-6-phosphatase. Fructose 2, 6-bisphosphatase is inhibited by increased fructose 2, 6-bisphosphate secretions thus resulting in gluconeogenesis.

1.4.1 Defects in insulin signal transduction

Identifying defects in the intracellular signaling cascade can be challenging as the defects can be at several levels. Defects in the IR have been implicated in insulin resistance. Mutations of the IR and some transcription factors like peroxisome proliferator-activated receptor-γ have been reported.[21] The location of some IR in caveolae is noteworthy. Caveolae microdomains and caveolin-1 are thought to be regulatory components in insulin signaling. Caveolae are invaginations found in the plasma membrane of different cell-types like adipocytes, myocytes and endothelial cells. They are rich in cholesterol and sphingolipids, just like lipid rafts, making them detergent insoluble and thus representing a class of detergent/carbonate-insoluble glycolipid (DIG) enriched microdomains. Caveolin-1, belonging to the caveolin gene family, is a cholesterol-binding integral membrane protein and a structural component of caveolae. Studies on rat adipocytes using immunogold electron microscopy established that the IR has high caveolae content. These studies indicated that GLUT4 translocation occurred in caveolin-rich membrane fractions. These observations were indicative of interactions between caveolae and caveolin-1

with IR, but their exact role in insulin signal transduction remains to be determined. However, mutations in caveolin-1 have been linked with severe insulin-resistance.[22] Internalization of the insulin-insulin receptor complex into endosomes and degradation of insulin by insulin degrading enzymes are also suggested to terminate the insulin-signaling cascade.[23] On the other hand, internalization of the receptor complex is thought to be favorable such that the receptor complex can access the downstream effectors and continue insulin signaling. However, the effects of receptor complex internalization are not fully understood and remain a topic of active investigation.[24] Components like protein-tyrosine-phosphatases namely protein-tyrosine-phosphatases-1B that interacts directly with the IR has been reported to be involved in insulin resistance. The absence of this phosphatase in protein-tyrosine-phosphatases-1B knockout mice resulted in an increased sensitivity to insulin in skeletal muscles due to increased phosphorylation of IR and IRS-1.[25] Some studies have indicated that release of free fatty acids and adipocytokines, like tumor necrosis factor-α in skeletal muscle, is linked with dysregulation of the insulin receptor resulting in insulin resistance. However not all researchers concur on the role of tumor necrosis factor-α in insulin resistance, and hence the topic is contentious.[17] Another kinase PKC, similar to PKB, is activated by insulin. PKC is thought to induce phosphorylation on residue Ser^{612} of IRS-1, thus inhibiting insulin signaling and resulting in insulin resistance.[26] Another study has linked increased phosphorylation of Ser^{307} on IRS-1 with tumor necrosis factor-α stimulation which

results in downregulation of IRS-1.[27] Yet another study associated increased Ser^{307} phosphorylation with insulin resistance, corroborating the role of Ser^{307} on IRS-1 in insulin resistance.[28] Identifying such defects in the intracellular signaling cascade is challenging but would provide an in-depth understanding of causes of T2DM and potential targets for designing new and improved drugs for the treatment of T2DM.

1.4.2 Available treatment options

Acute complications of diabetes include hypoglycemia and ketoacidosis, while chronic conditions include diabetic nephropathy, neuropathy resulting in amputations, coronary artery disease, stroke, hypertension and hyperlipidemia. Stringent lifestyle modifications, including diet and exercise, are key measures in management of diabetes but are not enough for effective control of the disease, and therefore use of anti-diabetic drugs becomes indispensable for prevention, management and treatment of patients.

The drug classes currently approved for treatment of T2DM include insulin, sulfonylureas, thiazolidinediones, glucagon like peptide-1 mimetics, amylin mimetics and dipeptidyl peptidase-IV inhibitors. Sulfonylurea derivatives are insulin secretagogues, which exert their effect of reducing blood glucose levels by stimulating insulin release from pancreatic beta cells. Thiazolidinediones are insulin-sensitizing, and they act by binding to a nuclear regulatory protein, peroxisome proliferator-activated receptor-γ, which is involved transcription of genes controlling glucose and fat metabolism.[29] Dipeptidyl

peptidase-IV inhibitors, as the name indicates, exert their action by inhibiting degradation of dipeptidyl peptidase-IV. This increases the level of incretin, glucagon like peptide-1 in the blood and improves glycemic control. Dipeptidyl peptidase-IV is also suggested to improve β-cell mass due to its mechanism of action.[30] Glucagon like peptide-1analogues and agonists are incretins that respond to increased glucose levels by secretion of more insulin. Incretins also inhibit glucagon secretion and thus maintain normal blood glucose levels.[31] Combination therapy and alternative medicinal sources, like plants, fungi and complex microbial secondary metabolites, have been explored as potential therapeutic agents for T2DM. There are a number of new classes of therapeutic agents, but none are optimal and none alone (other than insulin or insulin analogues) can achieve sustained satisfactory results. These agents are also associated with side effects and complications. On the other hand, the ability of IPGs to by-pass the defects of IR in the insulin signaling pathway that causes insulin resistance qualifies IPGs as potential anti-diabetic drugs. How would these IPGs then modulate the insulin-signaling pathway? Is there really a second messenger pathway that exists? If yes, at what stage do they converge? There have been numerous studies to seek answers to these questions as discussed below.

1.5 IPGs: second messengers of insulin signaling

Several reports in the literature propose an alternate pathway to the phosphorylation pathway.[32-34] In the second messenger pathway, the second

messengers or insulin mediators exhibit potential to intervene insulin's effect in parallel to the phosphorylation cascade pathway. Data indicating the existence of an alternate pathway was first reported by Larner and coworkers.[35] However, not much information was available on the identity of the second messengers until Saltiel and co-workers in 1986 reported purification methods for structural characterization of some second messengers. It was demonstrated that insulin stimulated hydrolysis of GPI molecules by PLC yields two mediators, IPG and diacylglycerol that act as the second messengers.[36] Some studies also indicated a possible role for the guanine nucleotide-binding protein known as the G-protein in production of the second messenger.[33] However, a number of questions remain unanswered. Controversy continues pertaining to questions about the GPI target molecule and its hydrolysis. Whether the GPI precursor is a GPI-anchored protein or a free-GPI is not clear. Furthermore, the cleavage of the GPI molecule can occur by either the PLC or possibly by PLD. If GPI hydrolysis occurs by PLC, is it due to G-protein stimulation or activation through tyrosine phophorylation of IR? Likewise, the structure and mechanism of action of G-proteins in relation to insulin remain to be established. Nevertheless, numerous in vitro and in vivo studies on the insulin mediator, IPG, from various sources indicated that IPGs are insulin-mimetic.

Although the second messenger pathway remains less understood, a lot of effort has been directed in understanding the mode of action of second messengers as related to the effects of insulin. At least two pathways are

proposed. One pathway hypothesizes that insulin binding activates PLC and that GPI hydrolysis occurs releasing IPG and diacylglycerol at the outer leaflet of the cell membranes. IPG enters the cells via an adenosine triphosphate-dependent IG transporter but bypasses the IR, exerting insulin-like effects by modulating proteins involved in the signaling pathway.[2] Another study showed that both natural and synthetic IGs in a cell-free assay could modulate pyruvate dehydrogenase phosphatase activity suggesting an intracellular role.[37] On the contrary, IGs also appear to stimulate cells without entering them, as demonstrated by the study on a fluorescent-labeled synthetic IG analogue. This IG analogue was found to stimulate lipogenesis in rat adipocytes without internalization in cells.[38] The second proposed pathway could help explain the above observation for the fluorescent-labeled synthetic IG analogue. This pathway, proposed by Muller and coworkers,[39] attributes IG's mode of action to the dynamics of plasma membrane microdomains. DIG microdomains are suggested to be heterogeneous, consisting of high cholesterol (hcDIGs) and low cholesterol (lcDIGs) regions. GPI-anchored proteins and the non-receptor tyrosine kinase (NRTK), $pp59^{Lyn}$ are found to be located in hcDIG enriched with caveolin and lipid-modified signaling proteins. Cytoplasmic signaling proteins with dually acylated long chain fatty acids interact with caveolin in hcDIG. A caveolin scaffolding domain has been shown to interact with high specificity with a caveolin-binding domain on signaling proteins.

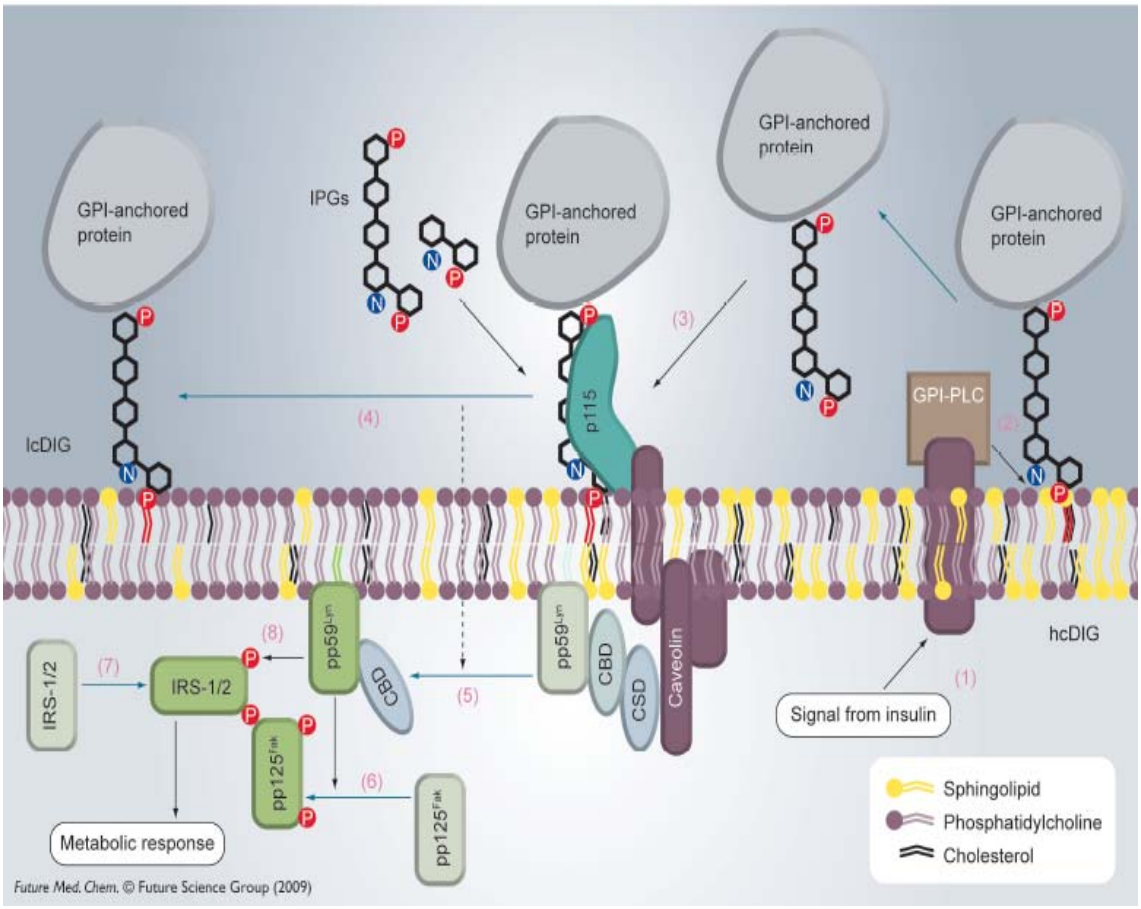

Figure 5. Schematic representation of IPGs and insulin signaling. (Reproduced from Future Medicinal Chemistry (2009), 1(1), 95-118 with permission of Future Science Ltd).

This type of interaction and another protein-protein interaction between flotillin and sorbin homology domain is thought to be important for recruitment of signaling proteins to DIG. A putative IG receptor for endogenous ligands such as GPI proteins/lipids has been reported. The IG receptor is a 115 kD polypeptide.[40] The proposed pathway is summarized in Figure 5.[41] Each step described below corresponds to the numbers indicated in Figure 5. (1) Insulin stimulates GPI-PLC. (2) This enzyme then lipolytically cleaves GPI-anchored

proteins (or free GPIs) on the outer side of the cell membrane. (3) The protein-IG conjugate (or IGs) competes with the GPI for the receptor, thus (4) dissociating the GPI-anchored proteins from the receptor, which translocate to an lcDIG microdomain. (5) Acylated NRTKs such as $pp59^{Lyn}$ on the inner leaflet are redistributed between hcDIG and lcDIG. This could be a repercussion of the changed lipid content brought by the translocation of GPI-anchored proteins to the hcDIG. (6) Kinase $pp59^{Lyn}$ activates $pp125^{Fak}$ which (7) recruits IRS protein for (8) phosphorylation by $pp59^{Lyn}$ at sites that are recognized by PI3K. This activates the phosphorylation cascade and serves as a point of covergence between the IG signaling pathway and the classical phosphorylation pathway.

1.6 Synthetic IPGs

IPGs, with their promising potential as therapeutic agents for T2DM treatment, have motivated various research groups to isolate IPGs from natural sources. Efforts are also being made to elucidate their structural composition and perhaps understand the mode of action. This is a daunting task as IPGs are heterogeneous. For example, IPG from rat liver and IPG from hepatoma cells contain *chiro*-inositol, while IPGs from rat liver, rat adipocytes, and BC3H-1 myocytes contain *myo*-inositol.[10-11, 42-43] In addition, the low amounts of isolated IGs from natural sources has contributed to the fact that the exact structure of IG has not been elucidated. A plethora of studies were therefore directed towards identifying the structural composition of IGs. The aim was to overcome the limitation of isolation of IPGs and alternatively rely on chemical synthesis to

produce IPGs of defined structure. The first definitive reports on GPI and IG structure were reported by Larner's[43] and Mato's group.[11] The structural IG components identified were a terminal inositol group, either *myo*-inositol or *chiro*-inositol,[11] an aminosugar glucosamine or galactosamine, and mannose residues with one or more phosphate groups. Based on metabolic labeling and degradation studies, it was also realized that the approximate molecular weight of 1400 Da for IGs made them closely related in size to the GPI membrane anchors.[10] GPI structure was explored as a model for designing IGs. d'Alarcao and co-workers[44] synthesized the first synthetic IG in 1992. It was an IPG-A pseudodissaccharide, compound **1**, which was reported to stimulate lipogenesis in rat adipocytes (Figure 6).

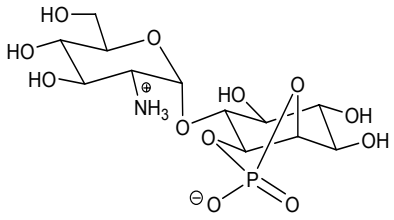

Figure 6. Structure of first synthetic IPG, **1**.

Three other compounds, synthesized at the same time, were shown to exhibit no insulin-mimetic activity. Based on these observations, the authors concluded that an amino-sugar in conjunction with *myo*-inositol-1, 2-cyclic phosphate was the minimum structural requirement for an IG to exhibit insulin-mimetic activity. This study pioneered the chemical synthesis of IGs, and

numerous research groups have now synthesized and evaluated IGs for insulin-mimetic activity.

A few years after the d'Alarcao paper [44], Muller and coworkers reported the synthesis and evaluation of 46 different IG analogues.[45] The most potent IPG, **41**, was a pseudohexasaccharide containing a *myo*-inositol-1, 2-cyclic phosphate, glucosamine, and four mannose residues with sulfate groups on two mannose residues (Figure 7).

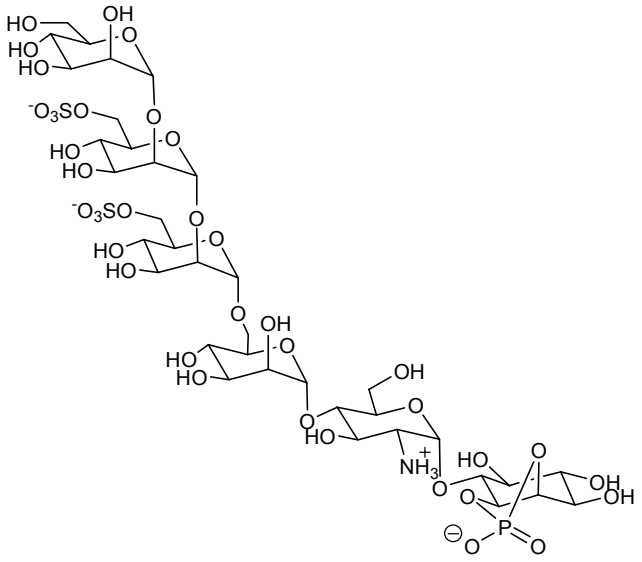

Figure 7. Structure of potent IPG, **41**.

The authors demonstrated that some synthetic IGs, in low micromolar concentration, could elicit insulin-mimetic activity up to 90% compared to insulin. The study further established that a minimum of one anionic group distal to the inositol core is required for high activity. Additionally, it was shown that the

anomeric configuration between glucosamine and the inositol core was insignificant, as compounds containing either α or β linkages were equally active. Although, the activity of compound **41** reported by Muller's group [45] was striking, the synthetic pathway was lengthy. A study by Chakraborty and d'Alarcao [46] reported a simpler, synthetic pathway to biologically active IG compounds. Two mannose residues in pseudotetrasaccharides **3** and **4** (Figure 8), instead of four in compound **41**, retained insulin-mimetic activity and stimulated lipogenesis in adipocytes.[46]

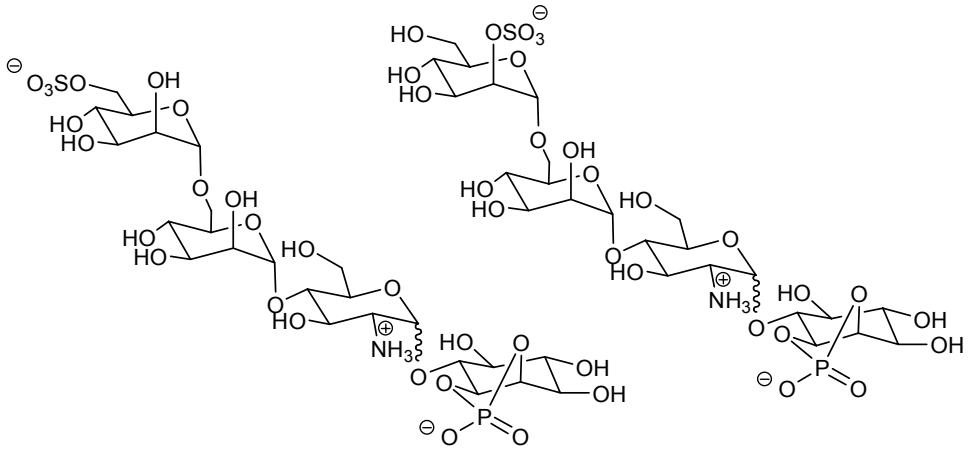

Figure 8. Structures of IPG **3α,β** and **4α,β**

The same group further reported synthesis of the non-hydrolyzable, palmitoylated IG, **IG-1**.[47] This synthetic IG showed the insulin-mimetic property of inhibiting lipogenesis with a reported activity of 24% MIR (maximum insulin response) with EC_{50} (effective concentration producing 50% cell kill) of 14 μM. This compound was also reported to have cytotoxic effects on some human

cancer cell lines. Additionally, it was realized that **IG-1** is highly selective in killing cancer cells. Based on these observations and comparing the activity of **IG-1** with known anti-cancer agents like resveratrol and butyrate which induce apoptosis in cancer cells, it was hypothesized that **IG-1** has anti-cancer properties and acts by reversing the Warburg effect, causing apoptosis in cancer cells. However, the presence of an ester linkage, which undergoes hydrolysis under physiological conditions, limited the use of **IG-1** as an anti-cancer agent.[47] To overcome this limitation, the same group [48] recently reported the synthesis of an ether analogue of **IG-1**, a non-hydrolyzable, palmitylated IG. Preliminary data on this IG suggest that it is considerably more stable than **IG-1** and exhibits similar biological activity.[48]

The potential of IPGs as second messengers cannot be stressed enough. The above two studies support the development of IPGs as a potential anti-cancer agent. Yet another study has implicated IPGs in transmembrane signaling in T lymphocytes.[49] Thus, it is evident that IPGs can have wider roles in signal transduction. However, the exact structure of IG, its mechanism of action, and its role in signal transduction need to be fully elucidated. A major challenge in doing so is the fact that the most active synthetic IPGs are also the most complex and, thus, involve lengthy synthetic schemes for preparation that make it difficult to obtain sufficient quantities for biological evaluations. Smaller and simpler IPGs showed a low insulin-mimetic activity as compared to active IPGs like compound **41**. d'Alarcao and coworkers reported an important and

interesting observation on a relatively simple fluorescent IPG derivative. In an effort to study IPG's mechanism of action, the researchers modified the first synthetic IPG from 1992, compound **1**, to make the fluorescent-labeled IPG, **17** (Figure 9).

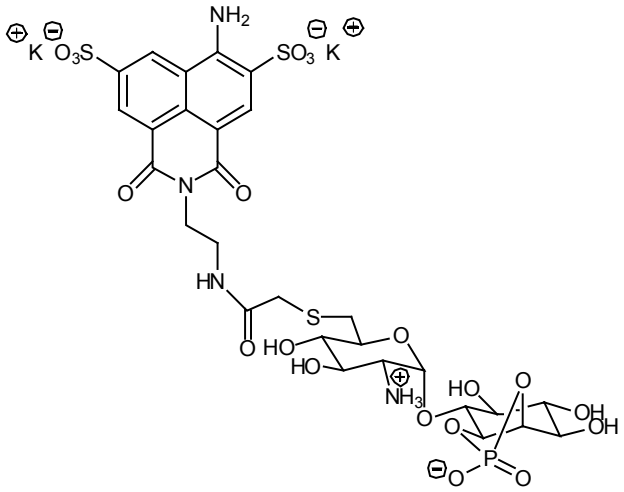

Figure 9. Structure of fluorescent-labeled IPG, **17**.

Compound **17** was prepared by coupling the 6-thiol-analogue of compound **1** with a commercially available iodoacetamide derivative of Lucifer yellow. The authors expected compound **17** to be weakly active but to serve as a good mechanistic probe. However to their delight, compound **17** was more active than compound **3**. It was found to stimulate lipogenesis with maximal activity of 47% relative to that of the maximal insulin response (MIR, defined as the stimulation by 5 nM insulin) and to have an EC_{50} of 12 μM.[38] The authors attributed the increased activity of compound **17** to the correct positioning of ionic groups on the IG and the Lucifer yellow fluorescent probe, a possible key

structural feature for the IGs to be active. Thus, it was clearly demonstrated that IG simpler analogues possessing the correct array of ionic groups even on a non-carbohydrate moiety like the Lucifer yellow chromophore could be biologically active. This study serves as a foundation for the proposed research.

CHAPTER 2

RESEARCH GOAL AND SYNTHETIC PLAN

2.1 Research goal

Synthetic IGs show great potential as therapeutic agents in the treatment of T2DM and cancer. However, most therapeutically active IGs are large complex compounds with lengthy and difficult synthetic pathways, which limit their therapeutic utility.

The primary goal of the proposed research is to synthesize a series of hybrid inositol glycan analogues (HIGAs) consisting of an inositol precursor coupled to a variety of non-carbohydrate moieties. The inositol core could be synthesized to accommodate cyclic phosphate and/or palmitate to form in analogues that resemble the biologically active IG structure. Compound **17**, a thiol analogue of compound **1** coupled to a non-carbohydrate moiety, is considered as the lead compound. As discussed in section 1.6 of chapter 1, the correct positioning of ionic groups on **17** is presumed to be the reason for the observed high activity. Based on the results from the studies conducted on compound **17**, it is hypothesized that some of the newly synthesized HIGAs could be biologically active.

The proposed shorter synthesis pathway of HIGAs will overcome the drawback of lengthy and complex synthesis of the current biologically active IGs.

The synthesized HIGAs will be evaluated for insulin-like activities such as stimulation of glucose transport, glycogen synthesis and lipogenesis.

2. 2 Synthetic strategy

Two strategies are proposed for the design and preparation of HIGAs.

2.2.1 Strategy 1

The first strategy is to use the 'Traceless Staudinger Ligation' method for synthesizing HIGAs. Traceless Staudinger ligation is a modification of the well-known Staudinger reduction reaction. The Staudinger ligation enables the formation of an amide bond between a phosphinoester (or phosphinothioester) and an azide group.[50] The by-product of the reaction, phosphine oxide, is expelled and does not form a part of the final product (contrary to the Staudinger reduction) and, hence, is known as a traceless method. An advantage of the traceless Staudinger ligation lies with the involvement of specific functional groups in the ligation process, the azide and the phosphine derivative. The mechanism of traceless Staudinger ligation allows a wide variety of modifications especially in the phosphine functional group. Additionally, the traceless Staudinger ligation reaction is highly chemoselective and can be carried out at room temperature in an aqueous environment. Furthermore, it is compatible with diverse functional groups, and therefore, is widely used in the field of organic synthesis and chemical biology. It is also used as a powerful tool in peptide ligations.[51]

The retro synthetic analysis utilizing this coupling strategy is shown in Scheme 1.[52-54]

Scheme 1. Synthesis of HIGA by traceless Staudinger ligation. [52-54]

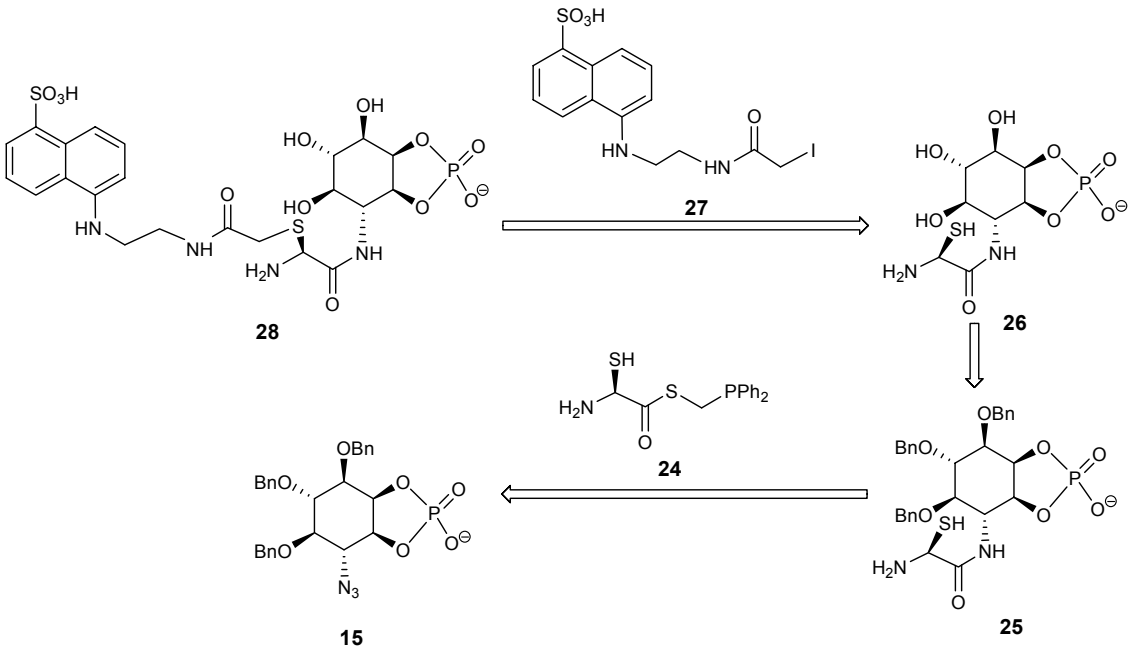

Compound **28** could be obtained by tethering the non-carbohydrate moiety, **27** to thiol containing **26**. Compound **26** could be obtained by deprotection of **25**, which in turn could be obtained by coupling **15** with **24** by the traceless Staudinger ligation method. Scheme 2 shows the retrosynthetic analysis for preparation of **24**.[55,56]

Compound **24**, a phosphinothioester, could be obtained from **23** by deprotection**,** which, in turn, could be obtained by esterification of **20** and **22**.

Compound **22** can be obtained by fluorenylmethoxy carbonyl chloride (fmoc) protection of the thiol and amino groups of commercially available cysteine. Compound **20** could be obtained in 4 steps from commercially available chloromethylphosphonic acid dichloride.[56]

Scheme 2. Synthesis of phosphinothioester.[55,56]

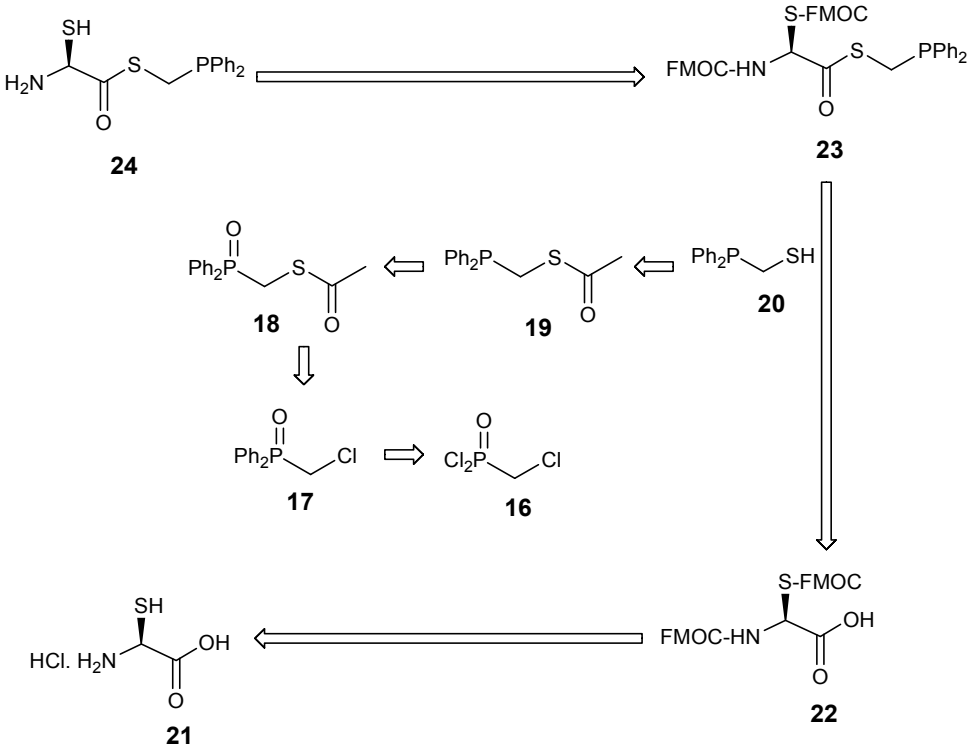

Cysteine was a reagent of choice for synthesizing phosphinothioester, **24**, for two reasons. Firstly, based on the data from several labs on IGs, it was observed that cyclic phosphate and a neighboring amino group are

characteristics of the most active IGs.[44, 45, 57] The amino group of cysteine would thus fulfill the requirement of a much-needed amino group as a structural component of HIGA. Secondly, the thiol group could serve as a linker for the non-carbohydrate appendages. Fmoc is a widely used protecting group in peptide synthesis and in organic synthesis for protection of amines. The advantages of the fmoc protecting group are its easy cleavage under mild basic conditions and its stability under acidic conditions.

Scheme 3 shows the retrosynthetic analysis for preparation of **15**.[55, 58-63] Compound **15** could be synthesized in 14 steps from commercially available D-xylose. D-xylose was chosen as the starting material due to its availability and cost. The overall yield of this set of reactions is about 15-20%, but the advantage is that the reactions can be executed on a larger production scale.

Scheme 3. Synthesis of **15**.[55, 58-63]

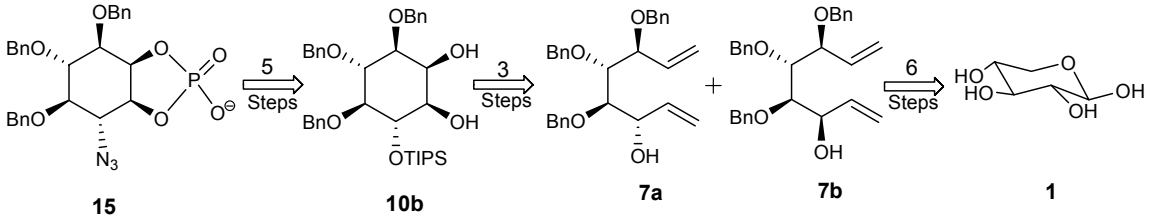

15 **10b** **7a** **7b** **1**

Based on strategy 1, the goal was to accomplish the parallel syntheses of **15**, **20** and **22**. Synthesis of **7a** and **7b** from **1**, towards the synthesis of **15**, was successfully achieved. Despite certain difficulties compound **22** was successfully

synthesized. Compound **17** and **18** were successfully synthesized from starting material, **16**, towards the synthesis of **20**. However, no success was achieved in synthesizing compound **19**.

While strategy 1 involved a novel synthetic route to **28**, it was lengthy, and a need for a shorter synthetic scheme was realized. Based on a further literature search an alternative, shorter synthetic scheme was designed.

2.2.2 Strategy 2

Strategy 2 was designed for a shorter synthetic route to HIGAs. The coupling strategy explored was the Huisgen cycloaddition reaction. With this strategy the target HIGA could be obtained in 15 steps versus 26 steps as in strategy 1.

The Huisgen cycloaddition reaction is a powerful coupling strategy that is very specific and is biocompatible with a variety of reactants.[64] It is a 1, 3-dipolar-cycloaddition reaction, which is categorized as a “click” reaction. There are variants of the 1,3-dipolar Huisgen cycloaddition, and the one employed for this strategy was the copper catalyzed azide-alkyne Huisgen cycloaddition reaction that generates a 1,2,3-triazole system. The copper catalyzed azide-alkyne Huisgen cycloaddition reaction requires simple reaction conditions, and starting materials that are readily available. These reasons led to the selection of this coupling method for strategy 2.

A retrosynthetic analysis for preparation of HIGA is shown in Scheme

4a and 4b.[52,53,65-70] Compound **16** could be obtained by coupling **15** (non-carbohydrate moiety) with **14**. Compound **14** could be obtained by global deprotection of **13**. Benzyl ethers are easy to remove and, hence, were employed as protective groups for alcohol and thiol groups in this synthesis. Compound **13** could be obtained by installing a cyclic phosphate on C1 and C2 of **12**. Compound **12** can be obtained by a "click" reaction between **11** and **10b**.

Scheme 4a. Synthesis of HIGA.[52,53,65-67]

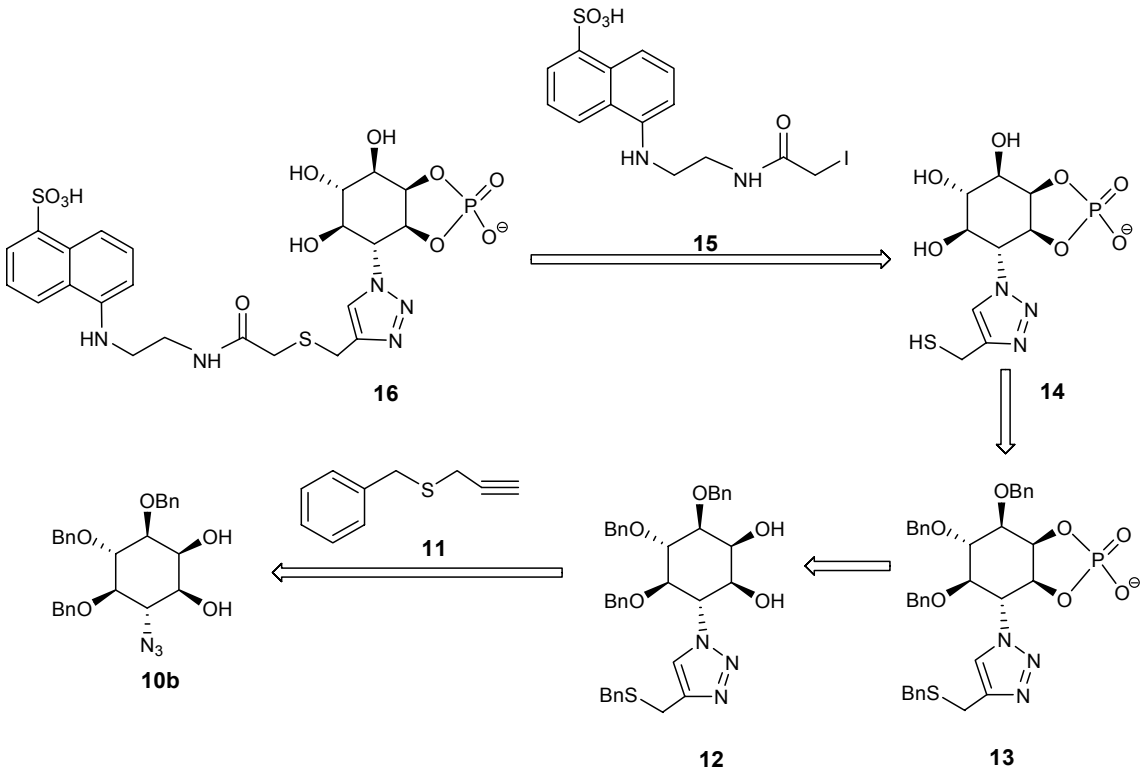

Compound **11** could be synthesized in one step from commercially available α-toluene thiol and propargyl bromide. Compound **10b** can be obtained after its separation from a mixture containing both undesired and desired diols, **10a** and **10b** respectively (shown in figure 12). Compound **10a** and **10b** could be obtained by dihydroxylation of **9** using catalytic amount of osmium tetroxide and *N*-methylmorpholine *N*-oxide. Although osmium tetroxide is highly toxic, volatile and expensive, it is one of the most efficient reagents for double bond dihydroxylation to give the corresponding vicinal diols.[71] *N*-methylmorpholine *N*-oxide is used as a co-oxidant to regenerate the catalyst, osmium tetroxide. Compound **9** could be obtained from **8b** by mesylation followed by nucleophilic substitution of the resulting mesylate with sodium azide (Scheme 4a). Compound **8b** could be obtained by resolving the diastereomeric mixture of **8a** and **8b** by flash chromatography. A Ring closing metathesis reaction on the mixture of **7a** and **7b** by using a first generation Grubbs ruthenium catalyst could produce a mixture of **8a** and **8b**. The first-generation Grubbs ruthenium catalyst has the advantage of commercial availability and stability, making handling of the catalyst easy. Compound **7a** and **7b** could be obtained in 6 steps from **1** (Scheme 4b). These reactions are well established by Prof. d'Alarcao's group.[62]

Scheme 4b. Synthesis of **10b** from **7a** and **7b.** [68-70]

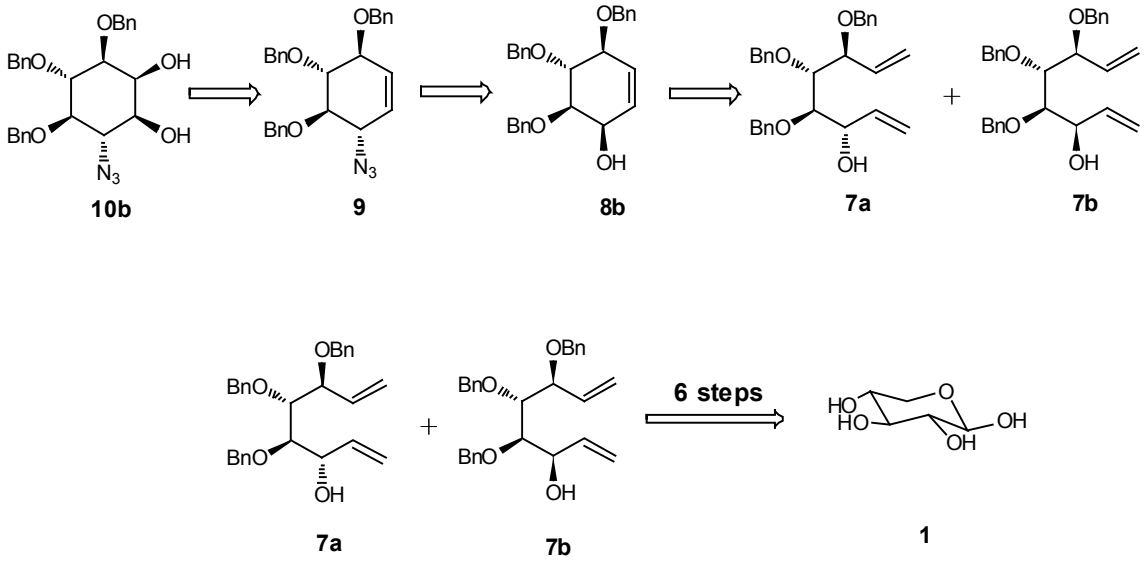

CHAPTER 3

RESULTS AND DISCUSSION

3.1 Synthesis of fmoc-protected cysteine, 22

Synthesis of **22** was attempted based on a literature procedure.[55] Cysteine hydrochloride was treated with fmoc chloride, and thin layer chromatography (TLC) indicated the complete disappearance of the starting materials. However, no product could be isolated. Neutralizing cysteine hydrochloride and raising the pH to 7 with 2 N sodium hydroxide before addition of fmoc chloride to the reaction mixture proved crucial, and compound **22** was obtained as a white foam.

3.2 Attempted synthesis of phosphinothiol, 20

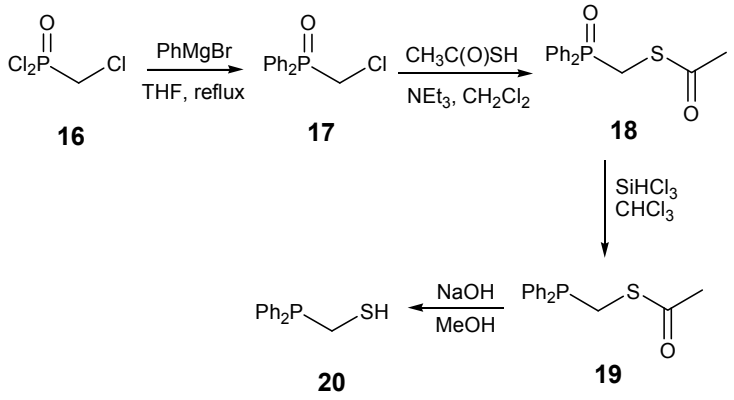

Figure 10. Synthesis of phosphinothiol, **20**.[56]

Synthesis of phosphinothiol was initiated by synthesizing compound **17** from the starting material chloromethylphosphonic acid dichloride, **16**, following a

literature procedure as shown in Figure 10.[56] Compound **18** was synthesized from compound **17**. A charcoal treatment for removal of inorganic impurities was reported in the literature, however a low yield of 13% was observed after the charcoal treatment. An improved yield of 48% was obtained after omission of the charcoal treatment step. An extraction process using aqueous sodium bicarbonate removed traces of acetic acid in the product. Synthesis of compound **19** from compound **18** was attempted twice, but no product was obtained. Trichlorosilane, a reagent required for the reaction, has a low boiling point of 31.8 °C and hence was difficult to be retained inside the reaction vessel. Attempts were then made to conduct the reaction in a completely sealed system (a pressurized vessel, a stainless steel bomb) and minimize the loss of trichlorosilane. In spite of all efforts, no product was obtained.

3.3 Synthesis of benzyl propargyl sulfide, 11

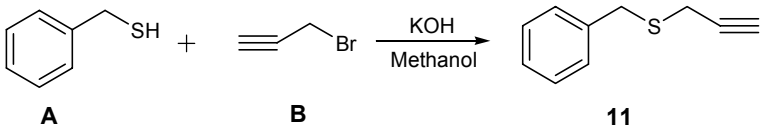

Figure 11. Synthesis of benzyl propargyl sulfide **11**.[66]

Compound **11** was obtained by propargylation of commercially available α-toluene thiol (**A**) with propargyl bromide (**B**). Product **11** was obtained as yellow oil with a good yield of 83%.

3.4 Synthesis of monosaccharide unit, 10a/10b

Compound **10b** was obtained in nine steps from D-xylose **1**. Compound **2** was obtained from **1** by the Fischer glycosylation reaction, an established reaction that has been well accomplished in the laboratory. Continued work with the Fischer glycosylation reaction in our laboratory revealed that yields of the reaction could be improved by varying the conditions of the reaction. Increasing the reaction time from 6 to 48h resulted in the increased formation of the pyranose form of the sugar and less of the furanose form of the sugar, as monitored by proton nuclear magnetic resonance (NMR). Benzylation of **2** gave the differentially protected compound **3**. Although the reaction was straightforward, certain difficulties were encountered. The dimsyl anion obtained from dimethyl sulfoxide and sodium hydride was partially soluble in the reaction mixture and, hence, had a tendency to form a solid that hampered the stirring process. The problem was overcome by use of a mechanical stirrer that ensured continuous mixing. Flash column chromatography was used to purify compound **3**, which was obtained in good yield. The next step was hydrolysis of the methoxy group at the anomeric position of **3** under acidic conditions. The reaction mixture was refluxed for 12h and filtered. The precipitate was collected by fractionation and crystallized from hexane-ether. Crystallization of **4** from hexane-ether as a solvent system proved to be a little complicated, and some amount of product was lost in the process. Recrystallization of **4** was attempted from methanol with the aim of improving the yield, and it was successfully

accomplished. A Wittig reaction was done on compound **4** to convert the hemiacetal to an alkene. The requirement of absolute anhydrous reaction conditions was achieved by thoroughly drying reagents utilized in the reaction. Triphenyl phosphonium salt was dried using a drying pistol for at least 24h. Compound **4**, the starting material for the reaction, was azeotroped 2-3 times from toluene to get rid of any trace of water. Only freshly distilled tetrahydrofuran was used in the reaction. Although extensive care was taken to retain anhydrous conditions for the reaction, the yield of the reaction, post purification, was only 35%. The amount of crude product obtained was more than the expected theoretical yield. This led us to consider that the loss of product could be occurring during the purification process. Instead of running flash chromatography for a longer period of time, purification of the crude was done by quickly passing the crude through a silica plug to minimize the contact of the crude with silica. This method of purification resulted in an improved yield of 55% of compound 5. Swern oxidation on compound **5** oxidized the alcohol on C 5 to an aldehyde compound **6**. The reaction was clean, and no purification was required. Compound **6** was then subjected to the Grignard reaction to give a mixture of isomers **7a** and **7b**. The use of different reaction conditions can vary the ratio of isomers **7a** and **7b**. Luchetti and co-workers in 2008 reported extensive work on optimizing these reaction conditions. According to the study, use of an additive, magnesium bromide ethyl etherate, in the Grignard reaction generated a higher ratio of isomer **7b**. This was attributed to the chelating ability

of the additive.[68] The effect of solvent on the ratio of **7a** and **7b** was also noteworthy and, with the aim of obtaining a higher ratio of **7b**, the ratio of tetrahydrofuran to dichloromethane used was 2:1 yielding a 2:1 ratio of **7a** to **7b**. The next step was ring-closing metathesis (RCM) on **7a** and **7b**. RCM is an intermolecular olefin metathesis that yields a cycloalkene. The first generation Grubbs catalyst was used for RCM to yield conduritols **8a** and **8b**. Purification by flash chromatography yielded the desired conduritol, **8b**. The next step was displacement of a hydroxyl group on C6 of **8b** by sodium azide to yield **9**, as shown in Figure 12.

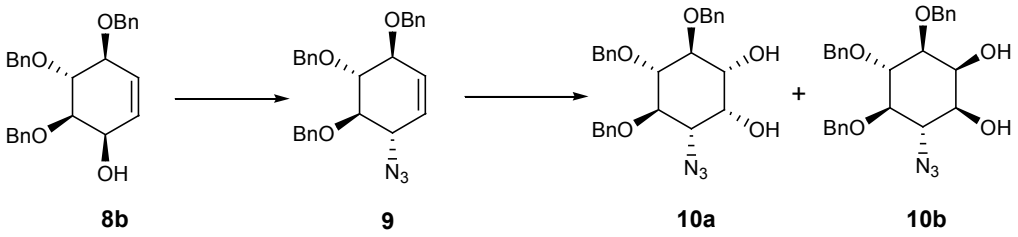

Figure 12. Synthesis of **10a/10b** from **8b**.

The aim was to synthesize **9** via mesylation followed by displacement of the resulting mesylate by sodium azide following a literature procedure.[69, 70] Accordingly, mesyl chloride was used as a source of the mesyl group, and an azido-alkene derivative was obtained as the product. Dihydroxylation of the resulting azido-alkene derivative was the next step. A mixture of two isomers (diols) was expected as the dihydroxylation product because of the alkene in **9**,

which is flanked by a bulky benzyloxy group on C3 trans to the azide group on C6. However, formation of only one isomer indicated some flaw during the azide displacement reaction. This problem was investigated by characterizing the intermediate mesylate product. Mass analysis revealed a mass corresponding to **8b** with a chloride group attached rather than a mesyl group. Based on these observations, it was hypothesized that the following sequence of steps occurred during the course of the reaction (Figure 13).

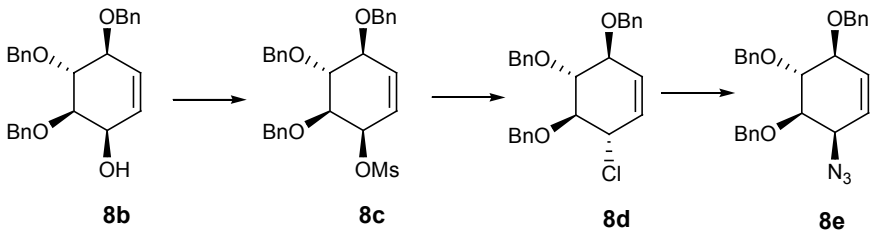

Figure 13. Synthesis of **8e** from **8b**.

Compound **8b** underwent mesylation to give **8c**. The reaction mixture at this stage had chloride anions (from mesyl chloride) that acted as a nucleophile, displacing the resulting mesylate to yield **8d**. A double displacement with sodium azide yielded **8e**, however with the opposite stereochemistry than the desired due to an additional S_N2 substitution by chloride anion. To circumvent this problem, mesyl anhydride was used as a mesylating agent, and **8b** successfully yielded compound **9** in the desired stereochemistry. Compound **9** was further

treated with osmium tetroxide in acetone-water (9:1) to yield a mixture of cis-dihydroxylated diols, **10a** and **10b**, with two OH groups 'down' and 'up', respectively. Preparative TLC yielded **10b** followed by **10a** in a 3:1 ratio.

3.5 Identification and characterization of diols 10a and 10b

The next task was to determine which isomer from the mixture of cis-dihydroxylated diols had two OH groups 'up' and which isomer had two OH groups 'down'. Since NMR spectra were ambiguous for characterization, each isomer was subjected to a deprotection reaction. Comparing the NMR spectrum of the resulting deprotected products to that of previously reported products,[72, 73] the identities of diols **10a** and **10b** were determined.

3.6 Synthesis of 12 by click reaction of 10b with 11

Following a literature procedure, a copper catalyzed Huisgen cycloaddition (click reaction) was done to afford crude **12**.[67] The reaction was quick and efficient, and disappearance of starting material on the TLC plates could be seen in less than 10 minutes. Visualization of the product on the TLC plates, however, proved tricky, as the product did not stain with p-anisaldehyde stain. Hanes-Isherwood stain and iodine were also tried, but neither proved efficient for visualization of the product. Thus, TLC plates were not stained, and ultraviolet illumination was chosen as the method of visualization. High-resolution mass spectrometric analysis and a proton NMR spectrum of the crude, proved its molecular mass to be **12**.

3.7 Synthesis of compound 16 from 12

The series of reactions to obtain **16** from **12** started by cyclic phosphorylation of **12** with methyl dichlorophosphate in pyridine following a known literature procedure.[65] Global deprotection of the phosphorylated product, **13**, by dissolving metal reduction using an established procedure,[53] yielded compound **14** which was kept under argon atmosphere. The final task was coupling of **14** with **5**-(amino)-naphthalene-1-sulfonic acid (1, 5-IAEDAN), **15**. 1, 5-IAEDAN is an organic fluorescent molecule and, hence, widely used as a marker in fluorescence microscopy. The advantage of using this reagent is that it has a high solubility in water above pH 4. Tris-HCl buffer (pH 7.5) was used as a solvent, and compound **14** was added to it followed by the fluorescent dye, **15**. The reaction mixture was protected from light by wrapping with an aluminum foil, as fluorescence of **15** is dependent on the environment and could be sensitive to light. The reaction was carried at under argon atmosphere to prevent air oxidation of the thiol group (present in **14**) to form disulfide bonds. Dithiothreitol or tris-(2-carboxyethyl) phosphine are reagents used to reduce disulfide bonds. However, earlier studies have reported low yields for coupling reactions when or tris-(2-carboxyethyl) phosphine was used for reducing disulfide bonds. The reason for this observation was attributed to the nucleophilic nature of or tris-(2-carboxyethyl) phosphine competing for the iodoacetamide.[38] Based on this observation, no disulfide reducing agent was utilized for this coupling reaction. The reaction mixture was stirred for 2h and fluorescent-labeled HIGA, **16**, was

obtained. High performance liquid chromatography (HPLC) analysis was done to characterize compound **16**. Initial results from HPLC and high resolution mass spectrometry analysis showed m/z ratio of 322.0865 (versus the calculated mass of 322.0443), confirming the molecular mass for dianionic compound **16**. Further structure elucidation of **16** would be done by ^{1}H NMR analysis.

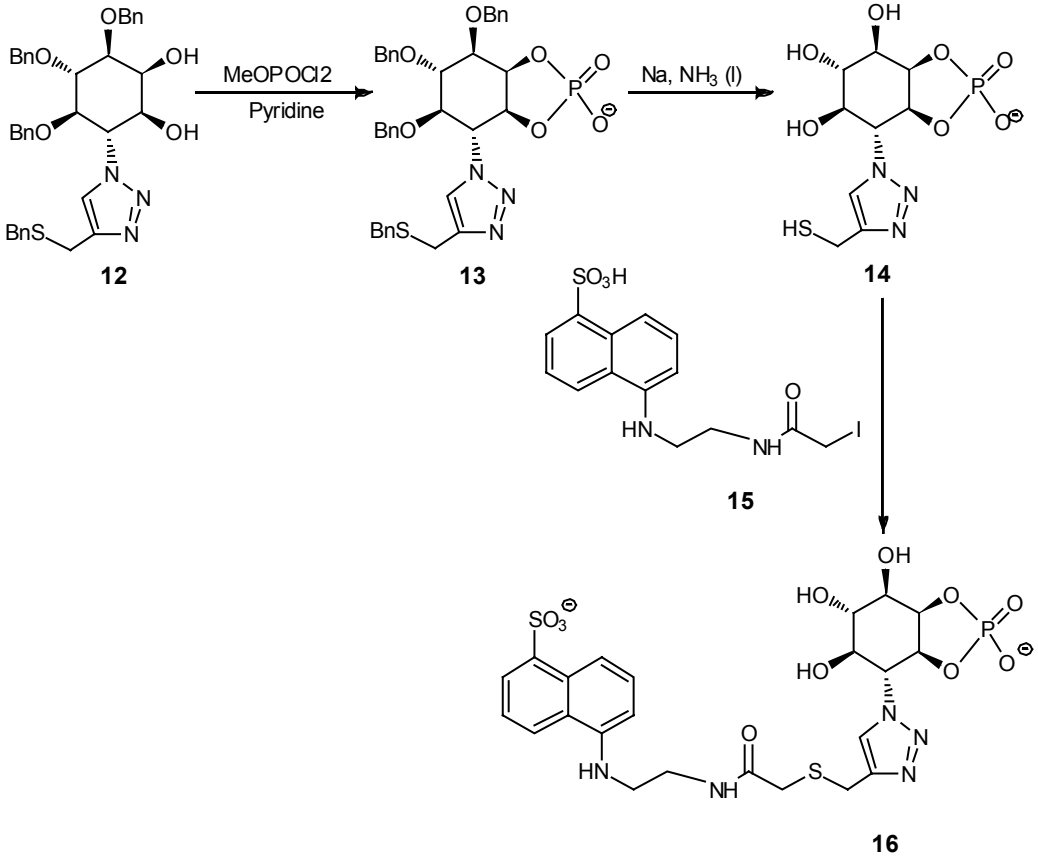

Figure 14. Synthesis of **16** from **12**.

CHAPTER 4

CONCLUSIONS AND FUTURE DIRECTIONS

The design objective for synthesizing HIGAs was to position ionic groups in approximate homology to the partially known IG pharmacophore. The challenge was to accomplish this task in a short and relatively simple synthetic pathway. The strategy used for this purpose was synthesizing the HIGA to consist of an inositol core covalently tethered to a variety of readily available non-carbohydrate moieties. Synthesis of one such HIGA (compound **16**) was successfully accomplished. Initial results of mass spectrometric analysis provide evidence for the structure of compound **16**. Further studies for structural elucidation of compound **16** are underway. In addition, we synthesized and characterized **8e**. A mixture of two dihydroxylated isomers (diols), **10a** and **10b** was successfully resolved and characterized. A click reaction of **10b** and **11** yielded **12**. Improving the yield of the reaction and use of a better visualization technique for **12** clearly need further development in the future.

Similar to compound **16**, more HIGAs where the inositol core is coupled to different non-carbohydrate moieties bearing maleimide or other fluorophore tags need to be synthesized and evaluated. HIGAs with fluorophore tags should be useful diagnostic tools for studying structure-activity relationship of IGs.

CHAPTER 5

EXPERIMENTAL PROCEDURES

All anhydrous reactions were performed under argon/nitrogen atmosphere. Reagents and solvents obtained from commercial sources were used without purification with the following exceptions. Methanol was distilled from magnesium metal and iodine crystals. Dimethyl sulfoxide was distilled from barium oxide. Methylene chloride was distilled at its boiling point. Pyridine was distilled from barium oxide or calcium hydride. TLC was performed on Baker glass backed silica gel plates (0.25-mm thickness). TLC monitored reactions and compounds were visualized by ultraviolet illumination and by using ethanolic solution of 2.5% p-anisaldehyde for staining. Purification of compounds was done by flash chromatography. In some cases preparative scale separations were performed on preparative TLC plates. Solvents were removed in vacuum on a Buchi rotary evaporator. NMR data were obtained on an Inova 400 MHz or 300 MHz spectrometer and the chemical shift is reported in parts per million (δ). Tetramethylsilane was used as an internal standard for all proton NMR spectra. High resolution mass spectroscopy (HRMS) data were obtained on a mass spectrometer using electrospray as the ionization method.

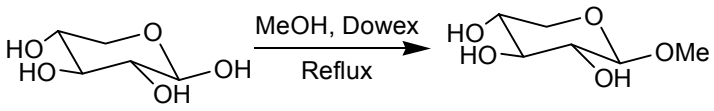

1 **2**

Methyl-D-xylopyranoside (2).[58] Distilled methanol (40 mL) was added to a flask containing D-xylose **1** (6 g, 40 mmol) and Dowex (2 g). The reaction mixture was refluxed until the TLC (acetonitrile-water, 85:15) indicated completion of reaction, approximately 20h. The resulting mixture was filtered over Celite, and the filtrate was evaporated to constant weight, producing 6.18 g (94% yield) of mixture of two isomers α and β methyl D-xylopyranoside **2**. ^{1}H NMR for mixture of **2α** and **2β** (400 MHz, D_2O): δ 4.13 (dd, *J* = 7.6, 2.8 Hz, 1H), 3.81-3.75 (m, 1H), 3.54-3.47 (m, 2H), 3.45–3.38 (m, 4H), 3.32–3.29 (m, 1H), 3.27-3.20 (m, 6H), 3.18–3.09 (m, 2H), 3.08–3.02 (m, 1H).

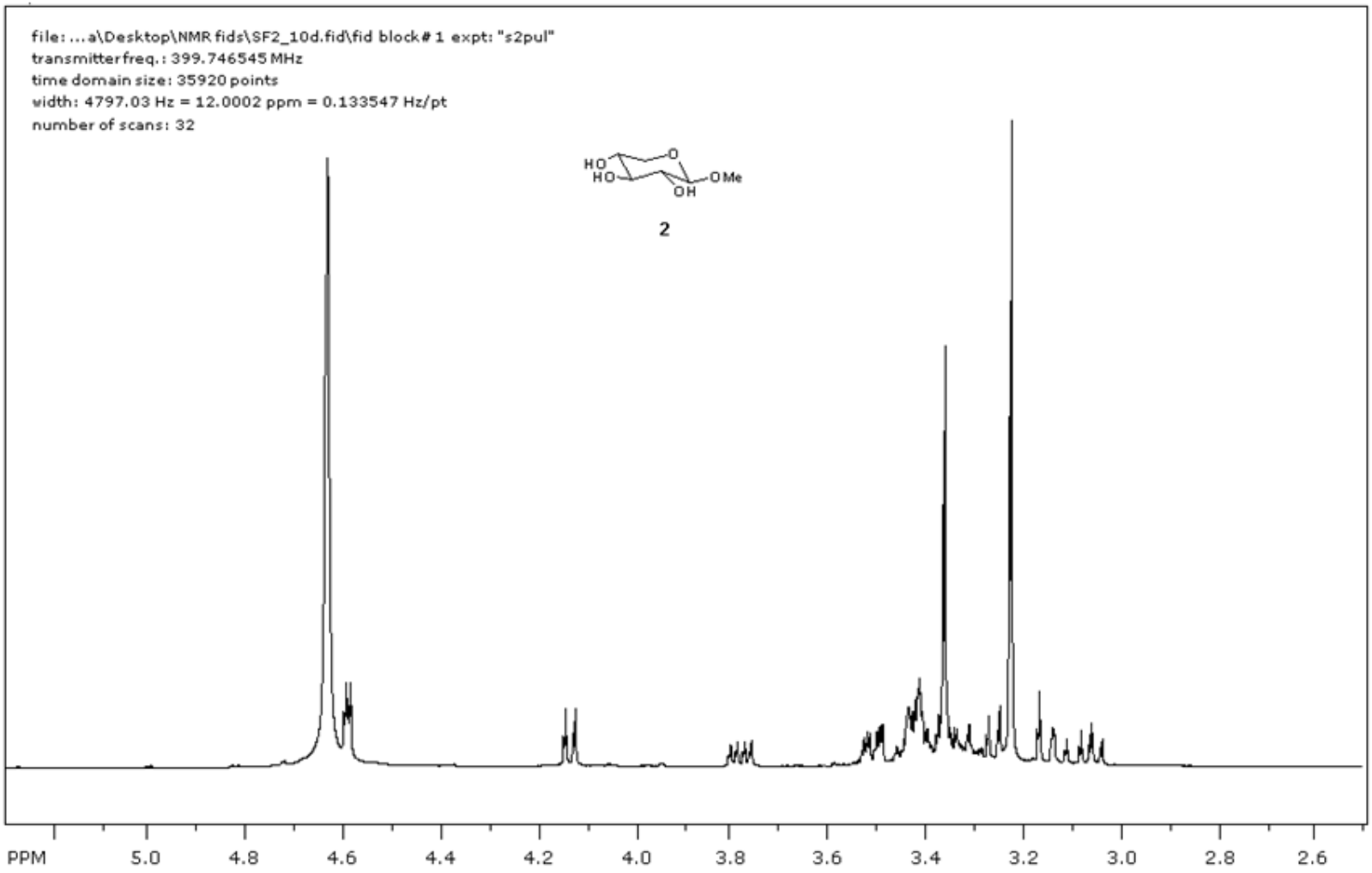

Figure 15. NMR spectrum for **2**

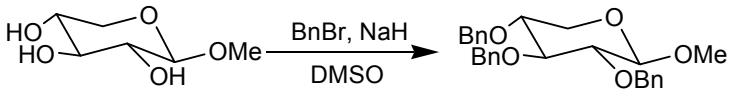

2 **3**

Methyl-2,3,4-Tri-O-benzyl-D-xylopyranoside (3).[58] Dimethyl sulfoxide (56 mL, 510 mmol) was added to sodium hydride (6.66 g, 540 mmol) under continuous stirring to produce the dimsyl carbanion. A solution of **2** (6.18 g, 120 mmol) in dimethyl sulfoxide (19 mL, 173 mol) was added dropwise to the reaction mixture over a period of 1h. A solution of benzyl bromide (21 mL, 550 mmol) in dimethyl sulfoxide (17 mL, 156 mmol) was added dropwise to the reaction mixture over a period of 3h and allowed to stir until completion of reaction, which was confirmed by TLC (ethyl acetate-hexane, 30:70). The crude was diluted with ice-cold water (200 mL), and the crude was extracted with diethyl ether (2 x 50 mL). The combined organic layers were dried over $MgSO_4$ and filtered. The solvent was evaporated, and the residue was purified by flash chromatography (silica, 1:4 ethyl acetate-hexane) to give 7.77 g (48% yield) of **3** as yellow oil. ^{1}H NMR for **3** (400 MHz, $CDCl_3$): δ 7.36–7.24(m, 15H), 4.76–4.61 (m, 7H), 3.92 (m, 1H), 3.82–3.74 (m, 3H), 3.54–3.50 (m, 1H), 3.43 (s, 3H).

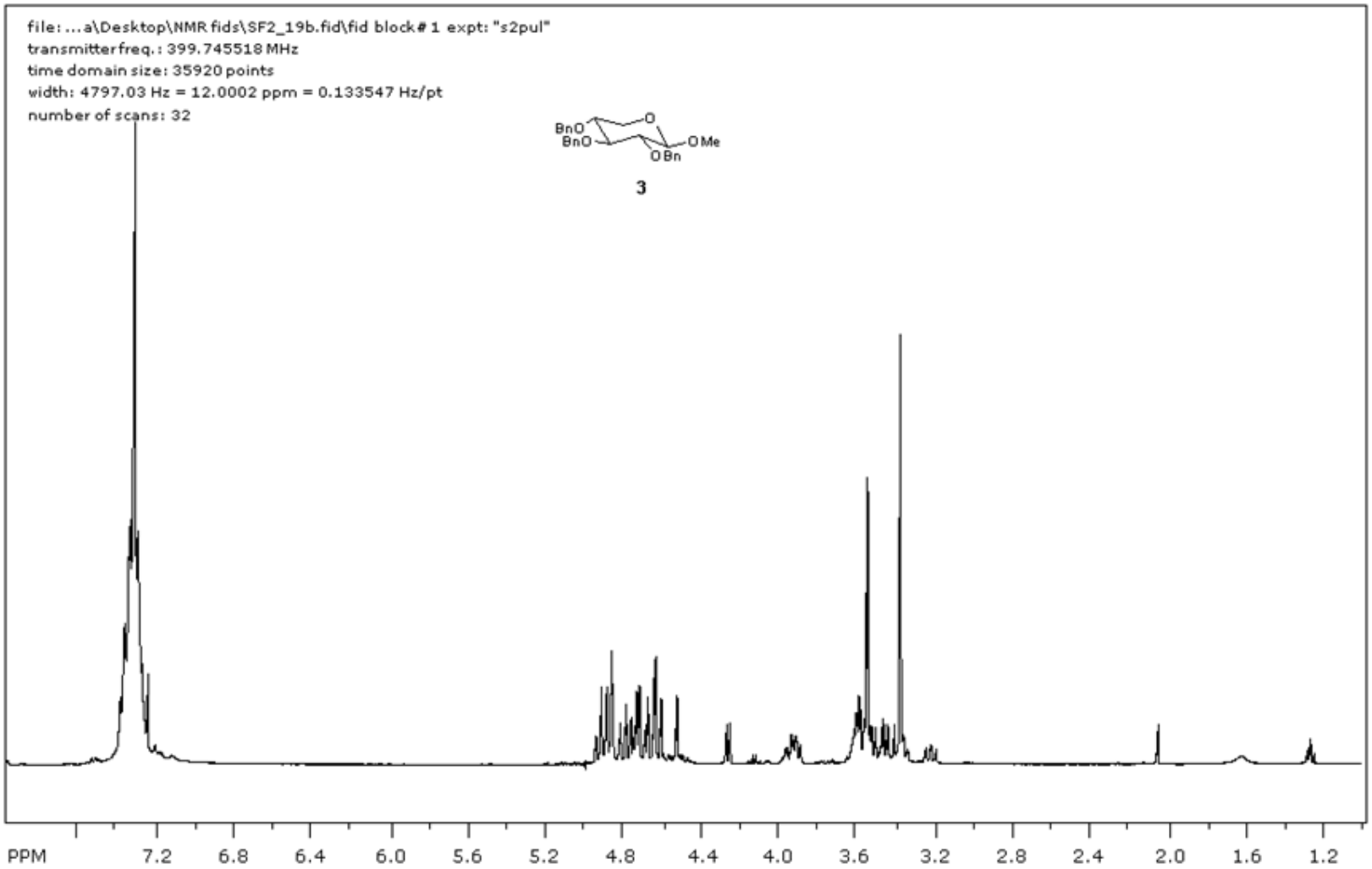

Figure 16. NMR spectrum for **3**

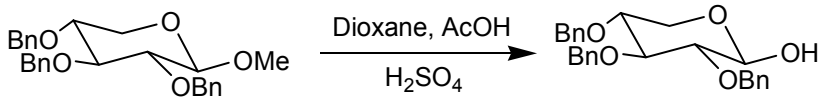

3 **4**

2,3,4-Tri-O-benzyl-D-xylopyranose (4).[59] D-xylopyranoside, **3** (6 g, 6.9 mmol) was dissolved in a mixture of 2 N sulfuric acid (17 mL), dioxane (18 mL, 102 mmol) and glacial acetic acid (19 mL). The reaction mixture was refluxed until TLC (ethyl acetate-hexane, 30:70) showed completion of reaction (approximately 20h). The crude was filtered and crystallized from hexane-ether (1:1) to obtain 5.53 g (95% yield) of **4** as white crystals. ^{1}H NMR for **4** (400 MHz, $CDCl_3$): δ 7.35–7.24 (m, 30H), 5.17 (m, 1H), 5.10 (m, 1H), 4.74–4.50 (m, 12H), 4.08 (m, 1H), 3.89–3.75 (m, 6H), 3.70–3.60 (m, 4H), 3.03 (m, 1H).

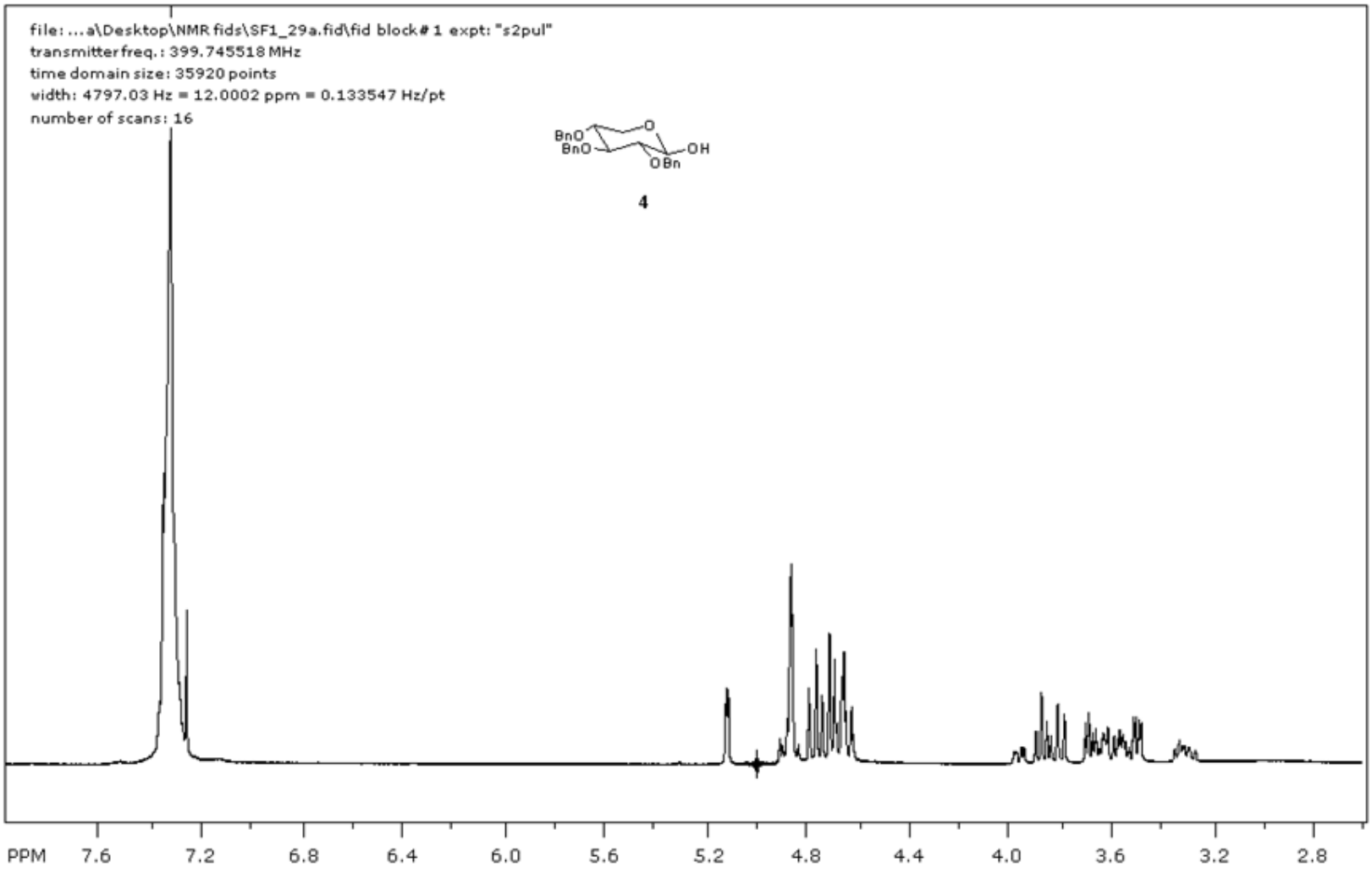

Figure 17. NMR spectrum of **4**

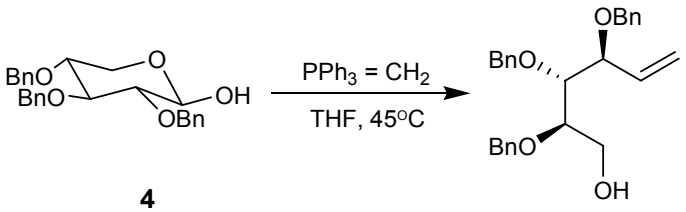

4 **5**

2(*R*),3(*R*),4(*S*)-Tribenzyloxy-5-hexene-1-ol (5). [60] To a suspension of methyl-triphenylphosphonium bromide (24.65 g, 69 mmol) in dry tetrahydrofuran (THF) (116 mL) added n-BuLi (55 mL, 65 mmol) was added dropwise at 0°C, and the reaction mixture was stirred for 2h. A solution of **4** (10 g, 23.78 mmol) in THF (73 mL) was added to the red reaction mixture at 0°C, and the reaction mixture was stirred overnight at room temperature and then at 45°C for 6h. Reaction mixture was then cooled to -10°C and filtered. NH_4Cl (100 mL of 1M aqueous solution) was then added, and the suspension was extracted with ether (2 x 100 mL). The combined organic layers were dried over $MgSO_4$ (s) and filtered. Flash chromatography (silica gel, ethyl acetate-hexane, 30:70) was done to purify **5** producing 5.43 g (55% yield). ^{1}H NMR for **5** (400 MHz, $CDCl_3$): δ 7.40 – 7.25 (m, 15H), 5.92 – 5.80 (ddd, 1H), 5.36 – 5.29 (m, 2H), 4.73 (s, 1H), 4.61 (d, 1H), 4.35 (d, 1H), 4.10 (m, 1H), 3.70 – 3.50 (m, 4H), 2.10 (br s, 1 H).

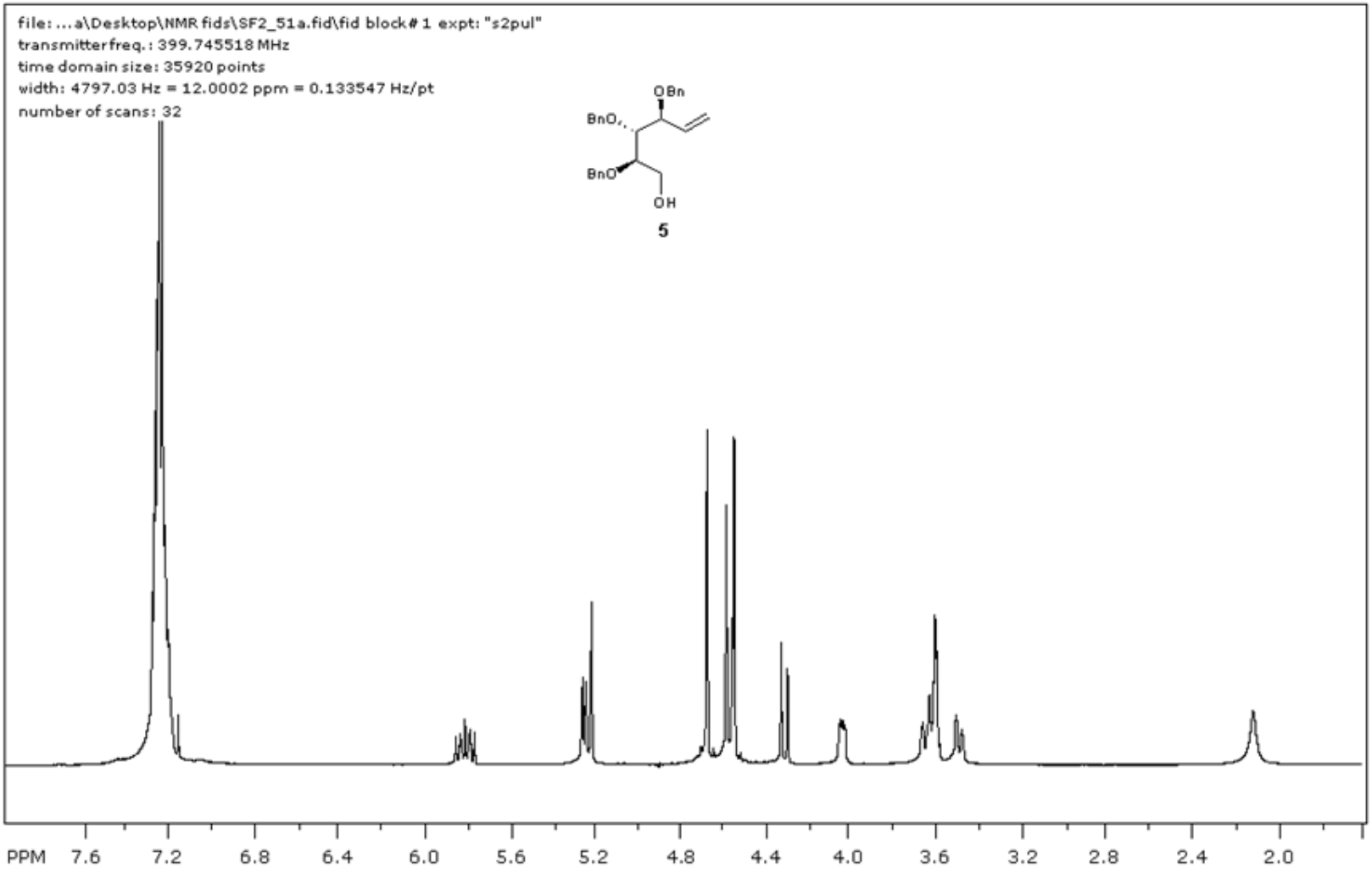

Figure 18. NMR spectrum for **5**

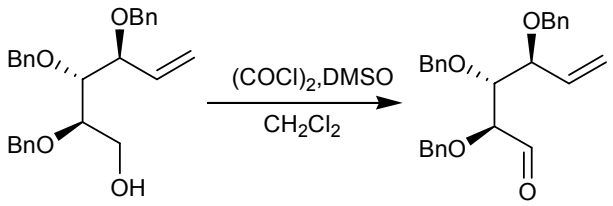

5 **6**

2(*S*),3(*R*),4(*S*)–Tribenzyloxy-5-hexenal (6).[61] Dimethyl sulfoxide (3.37 mL, 48 mmol) was added dropwise to a stirred solution of oxalyl chloride (2.03 mL, 24 mmol) in CH_2Cl_2 (40 mL) at -78°C. After 4 min, a solution of **5** (4.01 g, 9.6 mmol) in CH_2Cl_2 (25 mL) was added to the reaction mixture over 10 min, and the reaction mixture was stirred for 25 min at the same temperature. Triethylamine (10.6 mL, 77 mmol) was added within 4 min, the reaction mixture was stirred for additional 5 min and then warmed up to room temperature. Water was then added to the reaction mixture. The aqueous layer was extracted with CH_2Cl_2 (2 x 20 mL). The organic layers were combined and washed with NH_4Cl (2 x 30 mL, 1M aqueous solution), water (30 mL), brine (30 mL) and dried over $MgSO_4$. Crude **6** (3.99 g) was obtained after evaporation of the solvent. The material was considered sufficiently pure and was used in the next reaction without purification.

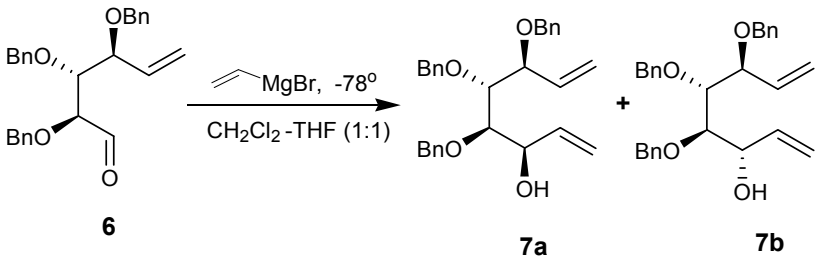

6 **7a** **7b**

3(*S*),4(*R*),5(*R*)-Tribenzyloxy-6-hydroxy-1,7-octadiene (7a and **7b).** [62]

A freshly prepared 2M solution of vinylmagnesium bromide in THF (64 mL) was added to a flask containing dry CH_2Cl_2 (20 mL) at -78°C. To the resulting solution, crude **6** (3.99 g, 9.5 mmol) in CH_2Cl_2 (0.27 mL) was added dropwise during 30 min. The mixture was stirred at that temperature for 3h, and then the reaction was quenched by addition of dry MeOH (10 mL). The mixture was warmed to room temperature and washed with NH_4Cl (80 mL, 1M aqueous solution), water (80 mL), and brine (80 mL) and dried over $MgSO_4$ to give 2.35 g (55% yield over two steps) of mixture of **7a** and **7b**. ^{1}H NMR spectrum of **7a** and **7b** was identical to that reported previously.[62]

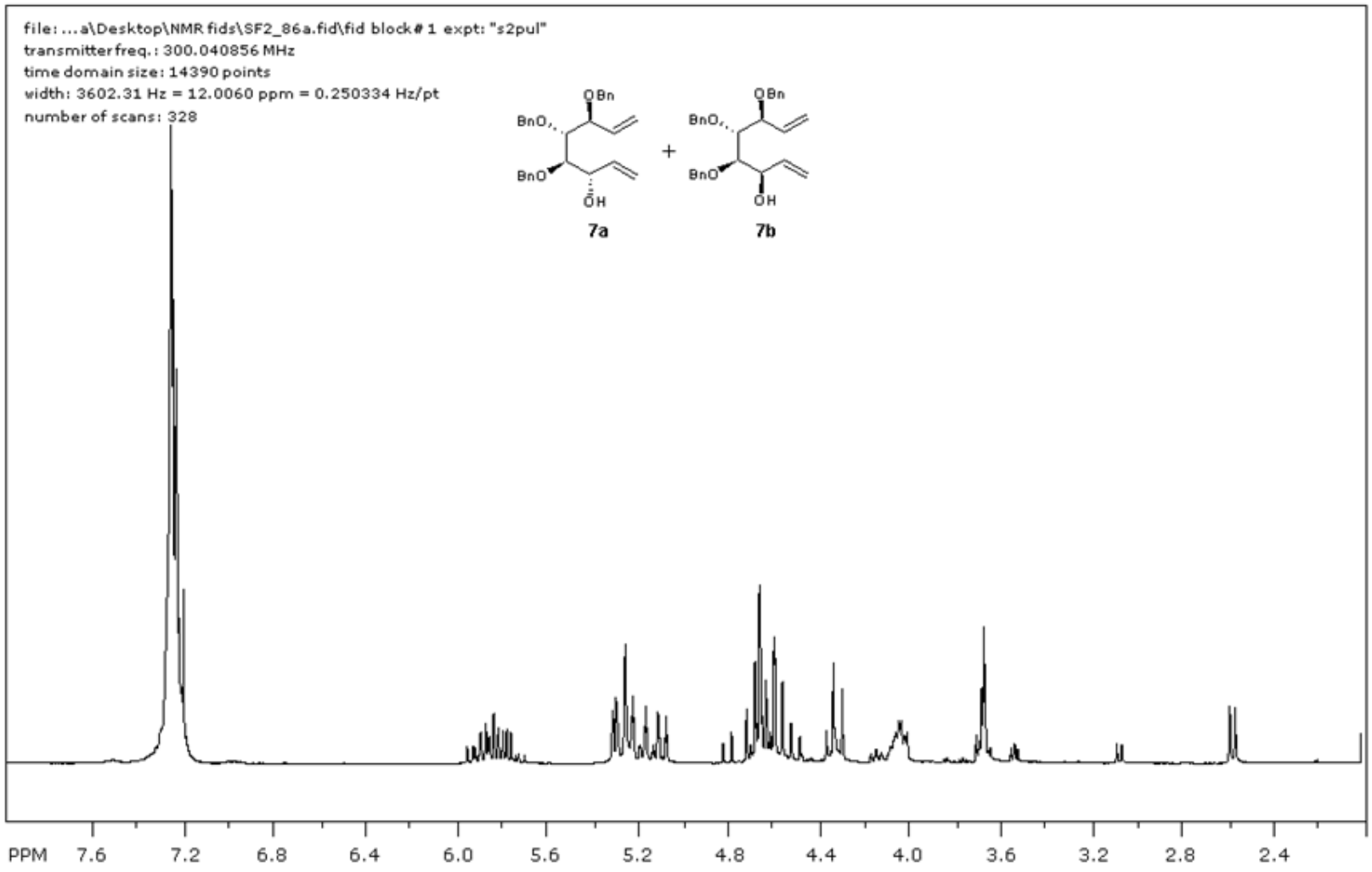

Figure 19. NMR spectrum for **7a** and **7b**

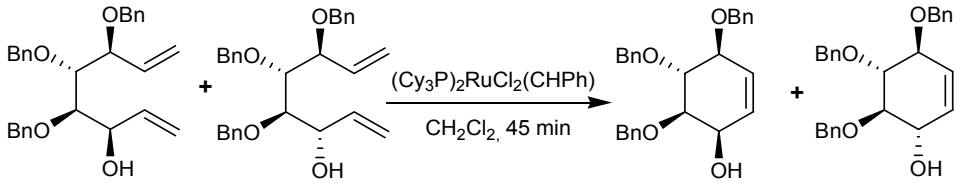

7a **7b** **8a** **8b**

3(*S*),4(*R*),5(*R*)-Tribenzyloxy-(6*R*)-hydroxycyclohexene (8a and **8b).**[68]

To a solution of **7a** and **7b** (1.16 g, 2.6 mmol) in CH_2Cl_2 (100 mL) $(Cy_3P)_2RuCl_2(CHPh)$ (0.14 g, 0.16 mmol) was added at room temperature. The reaction mixture was stirred for 30 min and opened to the atmosphere for 4h. The solvent was evaporated, and the crude was purified by flash chromatography (hexane: Et_2O, 1:1) to give 0.49 g (45% yield) of 8a followed by 0.41 g (38% yield) of **8b**. ^{1}H NMR for **8a** (400 MHz, $CDCl_3$): δ 7.35-7.25(m, 15H), 5.77 (d, *J* = 2.32 Hz, 2H), 4.94-4.66 (m, 6H), 4.18 (m, 1H), 4.02 (d, *J* = 7.24 Hz, 1H), 3.90 (dd, *J* = 2.84, 7.10 Hz, 1H), 3.46 (dd, *J* = 4.12, 9.72 Hz, 1H), 2.19 (bs, 1H). ^{1}H NMR for **8b** (400 MHz, $CDCl_3$): δ 7.35-7.25(m, 15H), 5.69 (m, 2H), 5.02 (d, *J* =11.3 Hz) 4.96-4.62 (m, 5H), 4.37-4.25 (m, 2H), 3.77 (dd, *J* =10.3, 7.3 Hz, 1H), 3.52 (dd, *J* = 10, 7.6 Hz, 1H), 2.16 (d, *J* = 3.3 Hz, 1H).

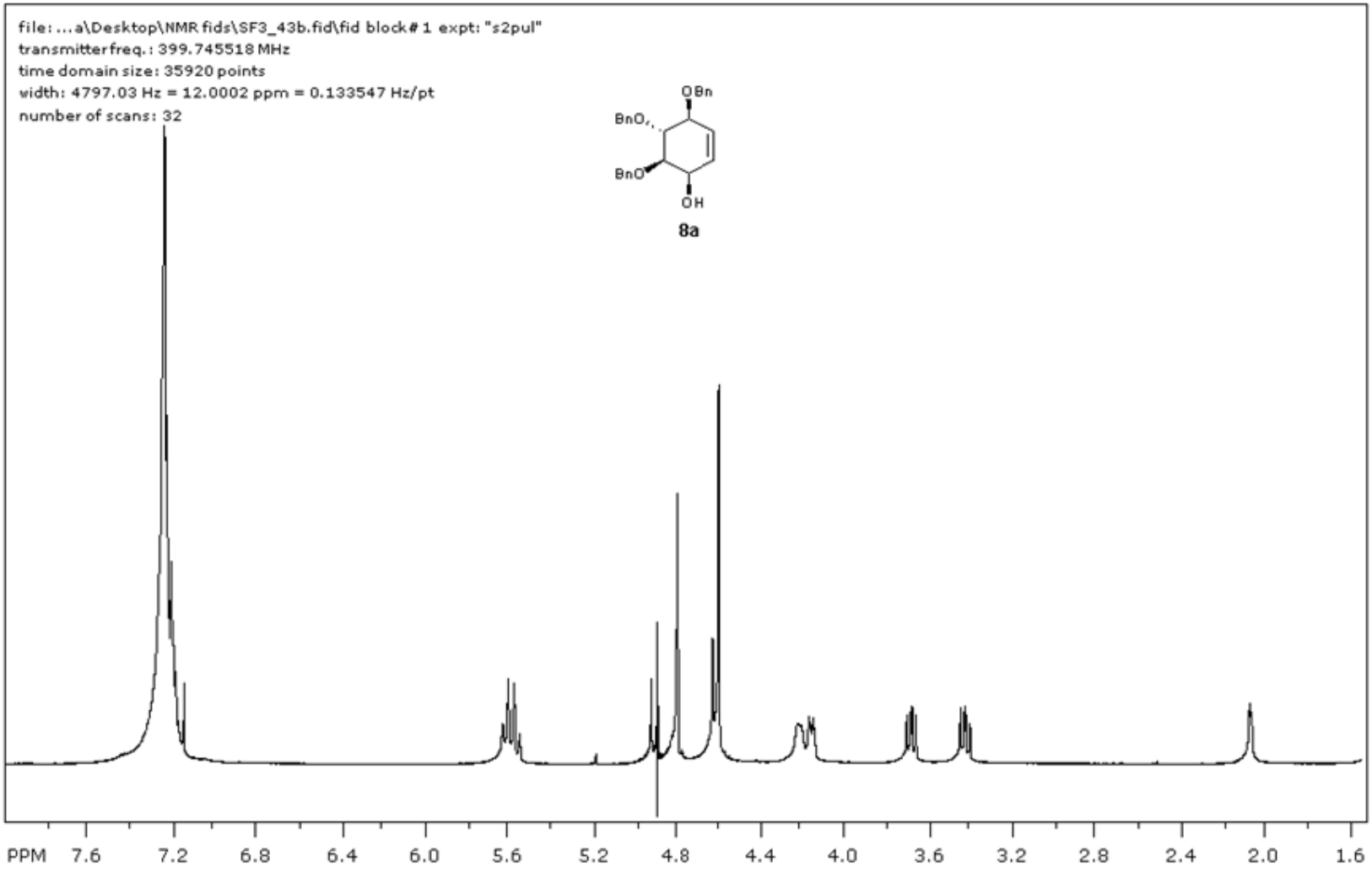

Figure 20. NMR spectrum for **8a**

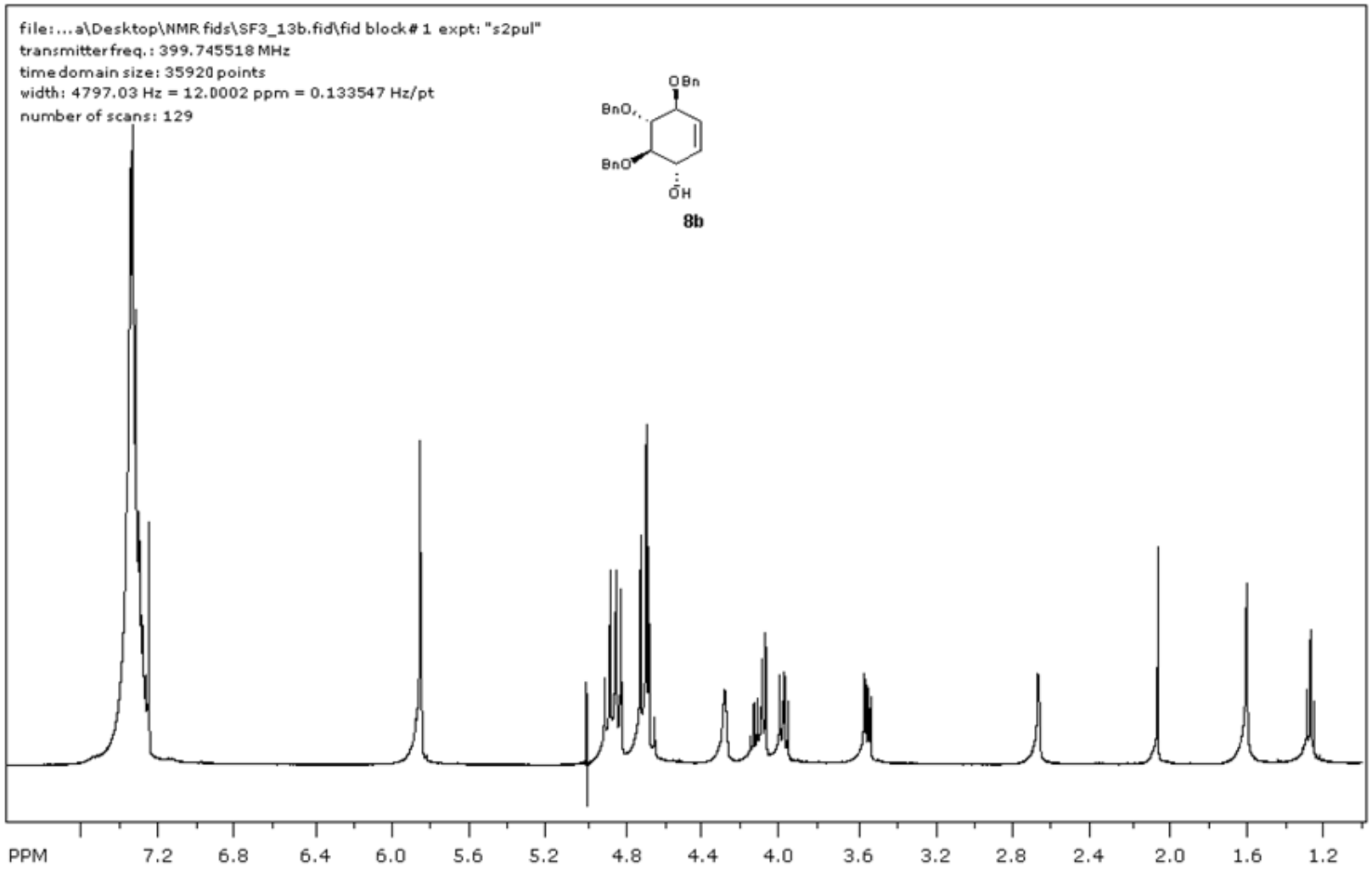

Figure 21. NMR spectrum for **8b**

8b **9**

Tri-*O*-benzyl-6-azidocyclohexene (9).[69,70] To a precooled (0°C) solution of **8b** (0.17 g, 0.40 mmol) in dichloroethane (3.4 mL), mesyl anhydride (0.076 g, 6.5 mmol) was added. Triethylamine (1.1 mL, 8.1 mmol) was added dropwise to the reaction mixture. The reaction mixture was stirred at 0°C until TLC indicated completion of reaction. The reaction mixture was diluted with ethyl acetate (60 mL) and washed with dilute acetic acid (2 x 6 mL) followed by a saturated solution of sodium bicarbonate (6 mL) and then dried over $MgSO_4$. The solvent was evaporated, and the crude residue was dried by coevaporation with toluene. The residue was placed in a flask to which sodium azide (0.13 g, 1.34 mmol) was added followed by dimethyl formamide (1.9 mL). The reaction mixture was stirred and heated at 85°C. On completion of the reaction, dimethyl formamide was removed by coevaporation with toluene. The residue was diluted with ethyl acetate, and the organic phase was washed with water (2 x 2 mL) and brine (2 x 2 mL), then dried over sodium sulfate. The solvent was evaporated, and the residue was purified by flash chromatography (hexane: Et_2O, 1:5) to give 0.072 g (41% yield) of **9**. ^1H NMR for **9** (400 MHz, $CDCl_3$): δ 7.35-7.25(m, 15H), 5.70 (d,

J = 10.4 Hz, 1H), 5.47 (d, *J* = 10 Hz, 1H), 4.94-4.66 (m, 6H), 4.11 (m, 2H), 3.70 (dd, *J* = 8, 10.4 Hz, 1H), 3.55 (dd, *J* = 8.4, 10 Hz, 1H).

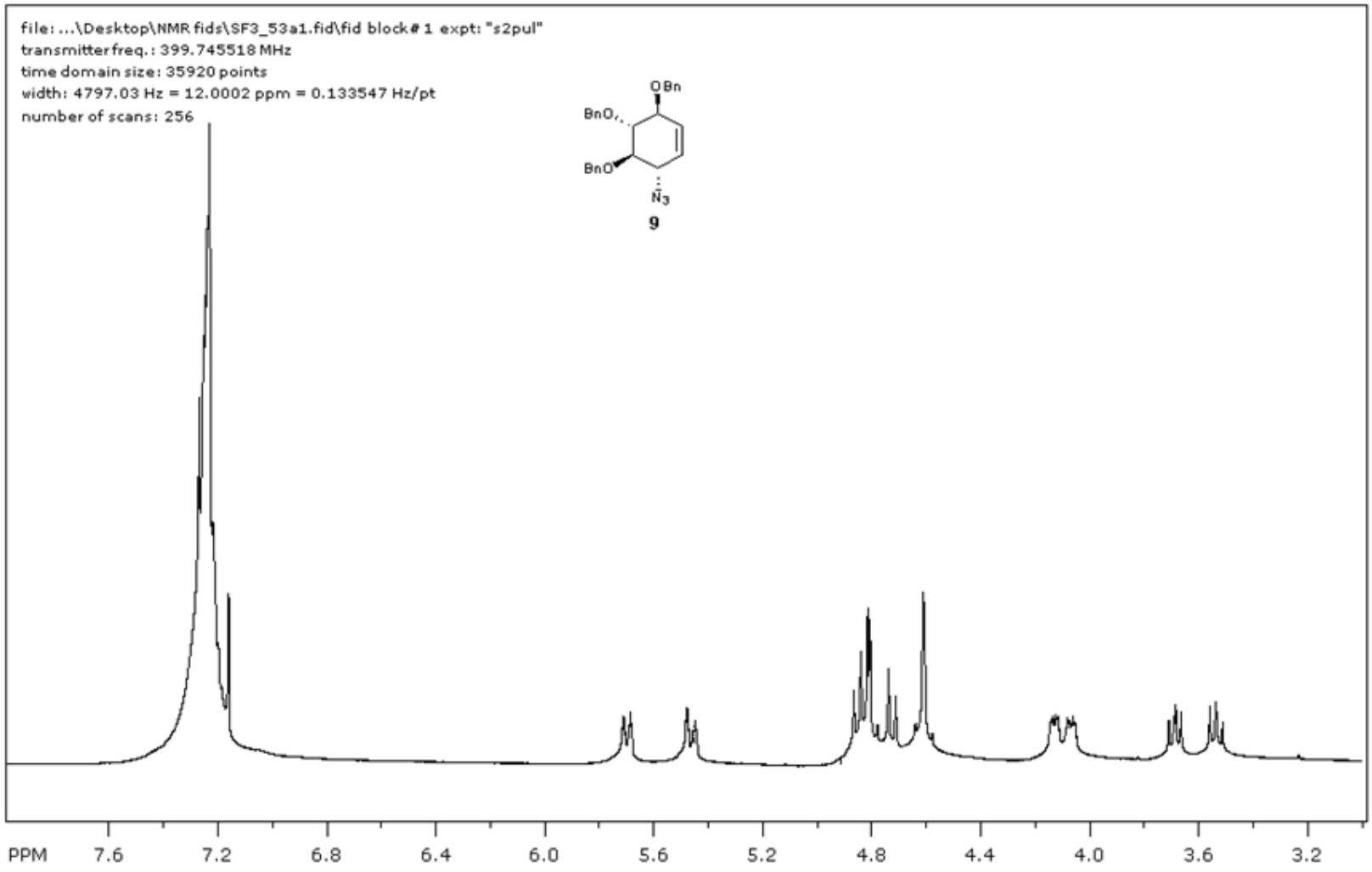

Figure 22. NMR spectrum for **9**

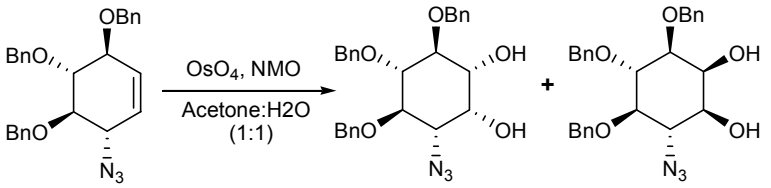

9 **10a** **10b**

Tri-*O*-benzyl-6-azido-deoxy-*myo*-inositol (10a and **10b).**[68] To a solution of **9** (8 mg, 0.018 mmol) in water: acetone (1:1, 0.73 mL) *N*-methyl morpholine *N*-oxide (2.4 mg, 0.068 mmol) was added followed by osmium tetraoxide (42.24 µL of 10 mg/mL of aqueous solution of osmium tetroxide). The reaction mixture was stirred until the reaction was complete and monitored by TLC. Diethyl ether was (4 mL) added to the reaction mixture, and the organic layer was washed with 10% aqueous sodium thiosulfate (3 mL) followed by water (3 mL) and dried over $MgSO_4$. The solvent was evaporated to give crude residue. Flash chromatography (silica gel, Hexane: ether, 1:1) gave 1.5 mg of **10b** followed by 0.5 mg of **10a** (23% yield). ^{1}H NMR for **10b** (400 MHz, $CDCl_3$): δ 7.35-7.25(m, 15H), 4.94-4.66 (m, 6H), 4.02 (d, *J* = 7.24 Hz), 3.90 (dd, *J* = 7.44 Hz, *J* = 7.44 Hz), 3.46 (dd, *J* = 4.12 Hz, *J* = 4.12 Hz), 2.69-2.49 (m, 1H).

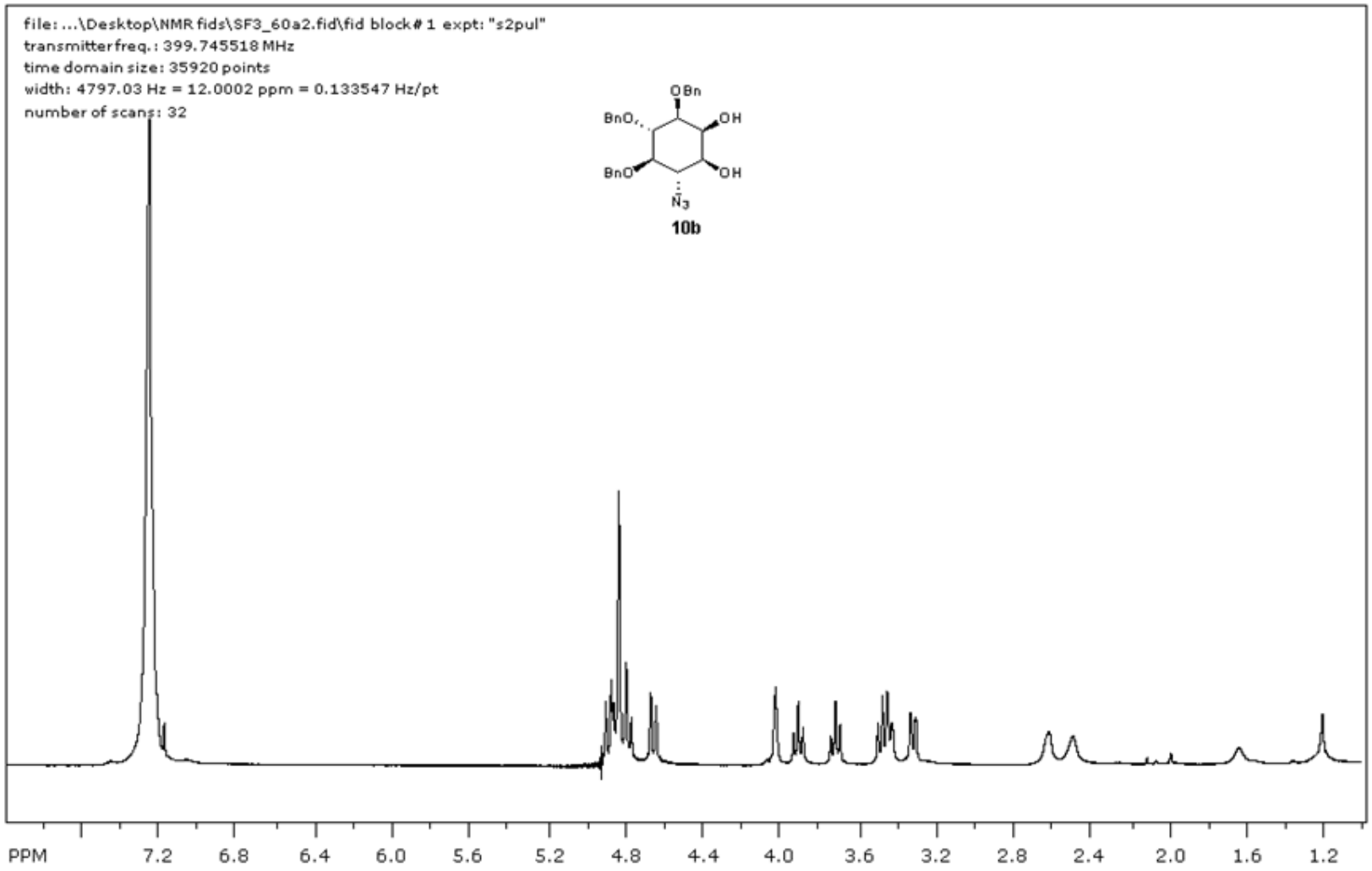

Figure 23. NMR spectrum for **10b**

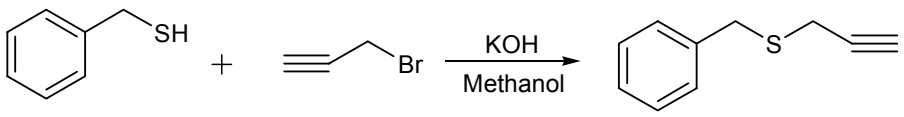

A **B** **11**

1-(Benzylthio)-2-propyne (11). [66] α-Toluene thiol **A** (5 g, 40.2 mmol) was dissolved in degassed methanol (0.5 M, 80.5 mL) at 0°C, and solid KOH (2.7 g, 48.3 mmol) was added to the reaction mixture. After 5 minutes, propargyl bromide **B**, 80% in toluene (6.5 mL) was added, and the reaction mixture was warmed to room temperature. TLC indicated completion of reaction in 3h. Methanol was removed from the reaction mixture under vacuum, and the residue was diluted with water (25 mL). The residue was extracted with ethyl acetate (2 x 50 mL) and dried over $MgSO_4$. The solvent was evaporated to give **11** (5.45 g, 83% yield) as yellow oil. The crude was then purified by flash chromatography. ^{1}H NMR for **11**(400 MHz, $CDCl_3$): δ 7.38 – 7. 27 (m, 5H), 3.88 (s, 2H), 3.08 (d, 2H, *J*=2.8 Hz), 2.31 (t, 1H, *J*=2.6 Hz).

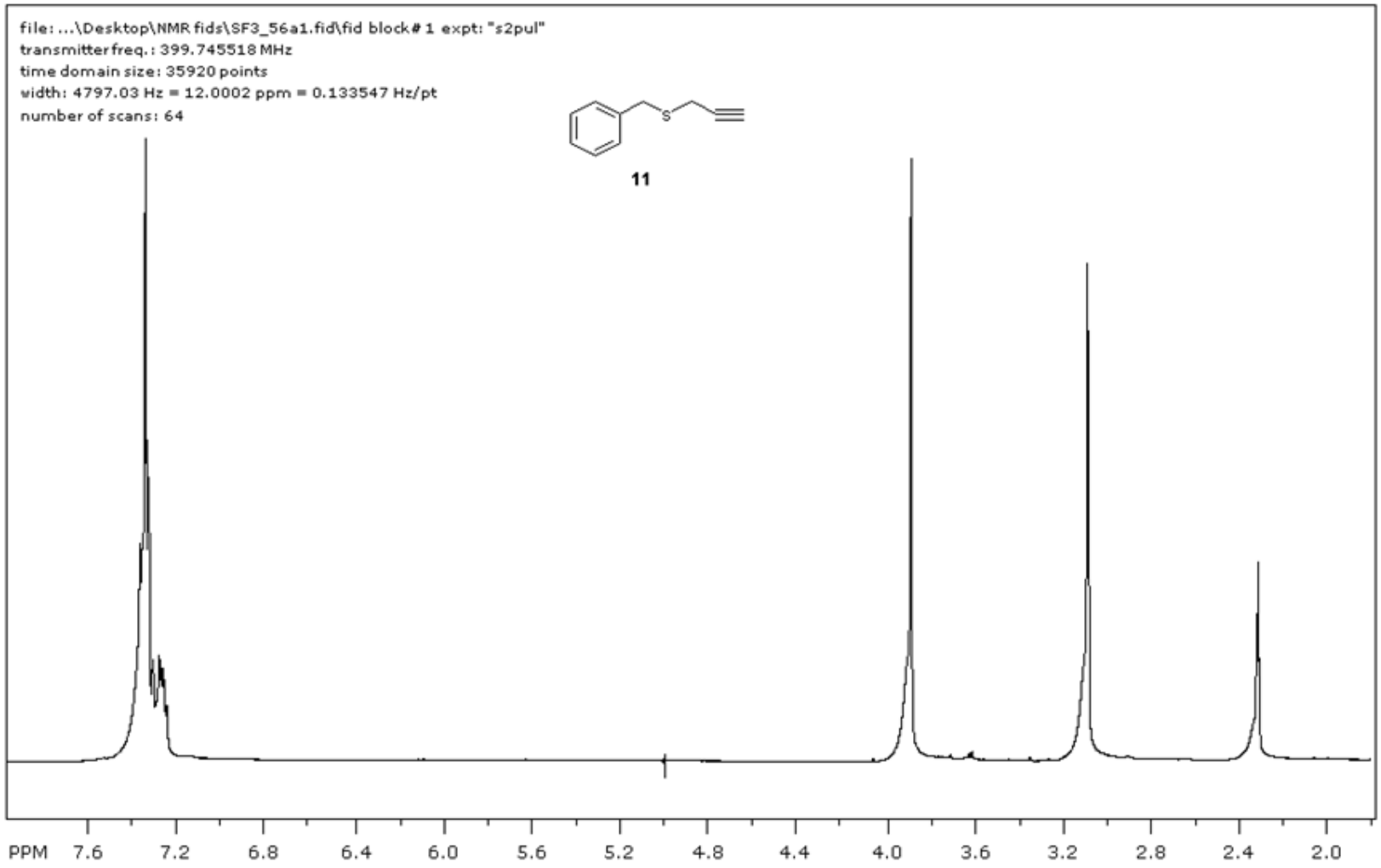

Figure 24. NMR spectrum for **11**

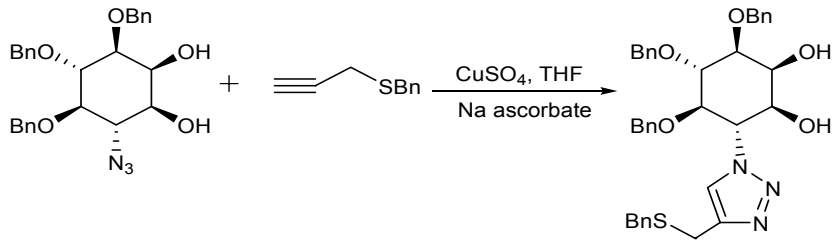

10b **11** **12**

Tri-*O*-benzyl-6-(4-benzylthiomethyl)-1, 2, 3-triazole-deoxy-*myo*-inositol (12).[67] To a solution of **10b** (5 mg, 0.0105 mmol) in THF (42 µL), propargyl sulfide (0.002 mg, 0.019 mmol) was added at room temperature. The reaction mixture was stirred, and copper sulfate pentahydrate (0.21 mg, 0.84 µmol) followed by sodium ascorbate (0.41 mg, 2.07 µmol) were added to the reaction mixture. The reaction mixture was stirred until TLC indicated complete disappearance of starting material. Water (0.3 mL) was then added to the reaction mixture, and the aqueous layer was washed with ethyl acetate (2 x 0.5 mL). The organic layer was washed with water (0.5 mL) and brine (0.5 mL) and dried over $MgSO_4$. The solvent was evaporated to give crude **12** (6.6 mg) as white solid. ^{1}H NMR for crude **12** (400 MHz, $CDCl_3$): δ 7.55 (s, 1H), 7.29 – 7. 20 (m, 32H), 7.14 – 7.12 (m, 3H), 6.88 – 6.86 (m, 2H), 4.95 – 4.74 (m, 8H), 4.64 (d, 1H, *J*=11), 4.56 (d, 1H, *J*=10.8 Hz), 4.36 (d, 1H, *J*=10 Hz), 4.28 (s, 1H), 4.20 (m, 1H), 4.08 – 4.04 (m, 1H), 3.93 – 3.88 (m, 3H), 3.72 (d, 2H, *J*=9.2), 3.59 (d, 4H, *J*=4.8 Hz), 3.47 (s, 1H) 3.34 (d, 1H, *J*=10.8 Hz), 2.40 - 2.35 (m, 2H). HRMS (ESI): m/z calculated for $C_{37}H_{39}N_3O_5S$: 638.2688. Found: 638.2684.

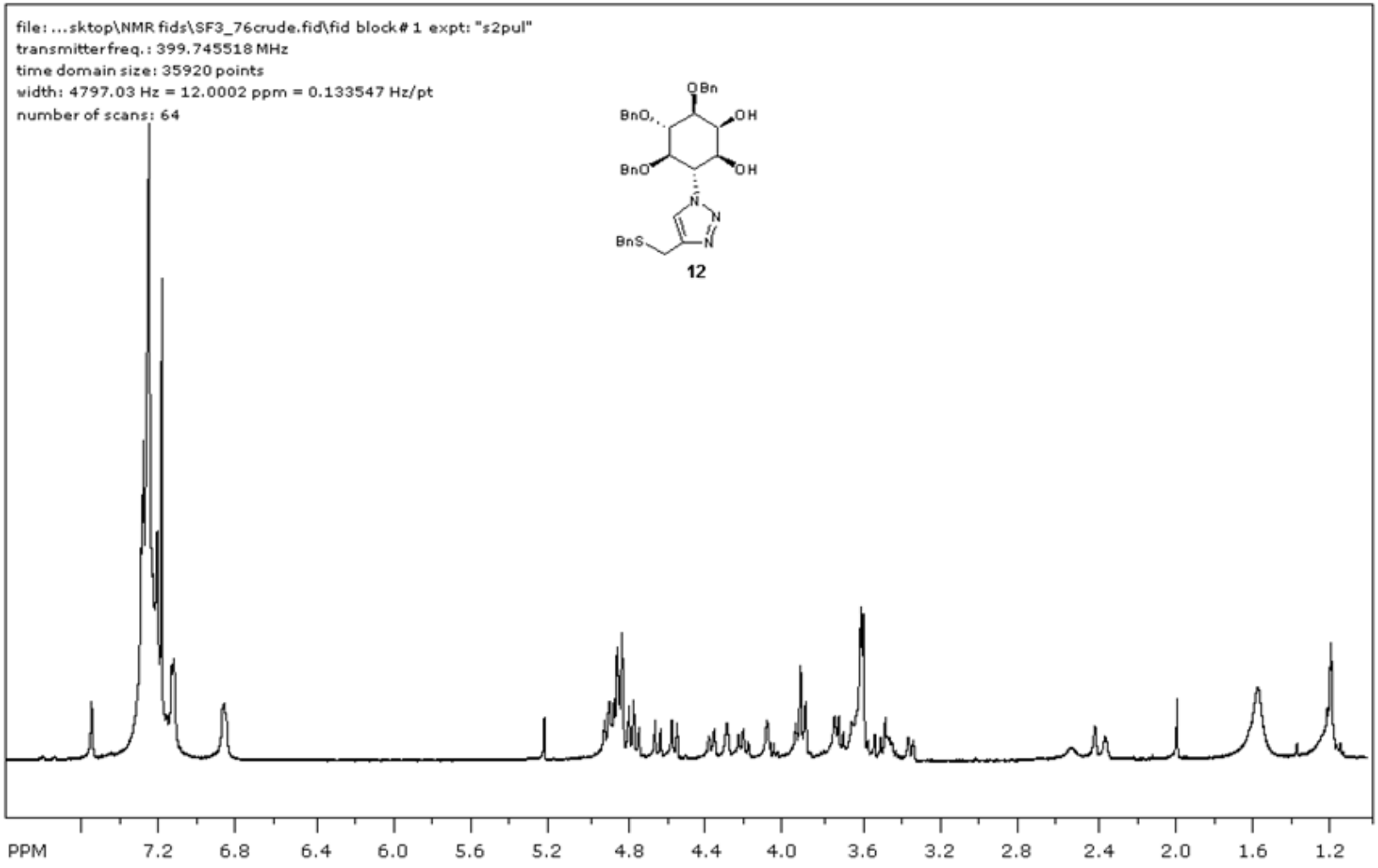

Figure 25. NMR spectrum for crude **12**

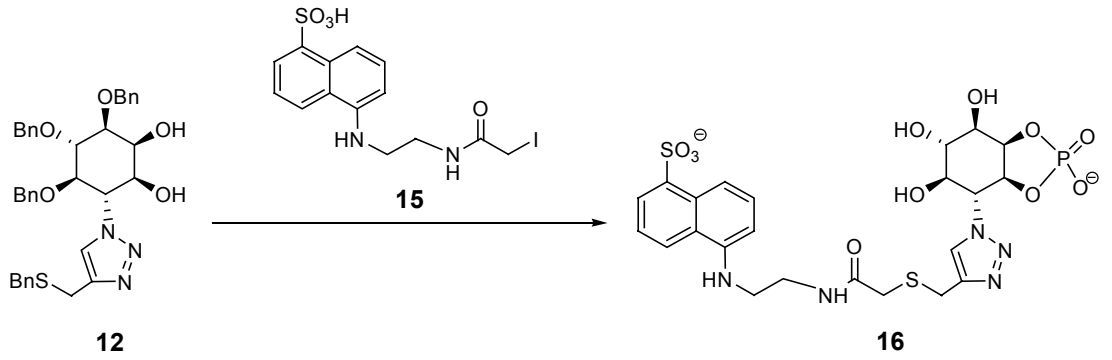

6-[4-{5-(methylthio[acetylamino]-ethylamino)-napthalene-1-sulfonate}-1, 2, 3-triazole]-6-deoxy-*myo*-inositol-1,2-cyclic phosphate (16).[67] $MeOPOCl_2$ (500 μL) was added to pyridine (5 mL). The reaction mixture was stirred at room temperature for 30 min. To a solution of **12** (6.6 mg, 0.0105 mmol, assuming 100% yield) in pyridine (70 μL), the above freshly prepared reagent (107 μL) was added, and stirring was continued at room temperature until TLC (silica, 1:1:1 $CHCl_3$-diethyl ether-MeOH) indicated completion of reaction. The reaction was quenched by addition of $NaHCO_3$ (0.2 mL), and the resulting mixture was co-evaporated from heptane. The resulting crude was further co-evaporated with toluene and then transferred to a flask containing THF (1.78 mL) under argon. In a separate flask NH_3 (5.35 mL) was condensed at -78°C and Na (14.28 mg) was added. After 15 min when the blue color persisted, the crude dissolved in THF was added dropwise, and the reaction mixture was stirred at -78°C for 15 min and quenched with solid NH_4Cl (32 mg) at -78°C. Methanol was added once the blue color had disappeared, and the reaction mixture was warmed to 20°C. The

solvent was evaporated to give the crude product. Tris HCl buffer (pH 7.5, 1 mL) was added to the resulting crude under argon. The reaction mixture was allowed to stir, and 1, 5-IAEDAN (4.56 mg, 0.0105 mmol) was added. The reaction mixture was stirred for 2 h at room temperature to yield compound **16**. HRMS (ESI): m/z calculated for $C_{23}H_{26}N_5O_{11}PS_2^{2-}$: 322.0443 Found: 322.0865.

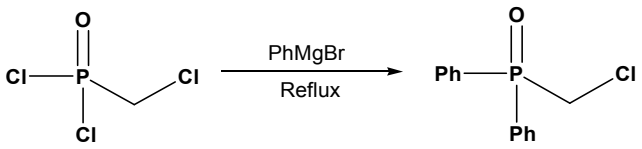

16 **17**

Phosphine Oxide (17).[56] Chloromethylphosphonic dichloride (0.12 mL, 1.19 mmol) was dissolved in freshly distilled THF (2.4 mL). A solution of phenylmagnesium bromide (1.0 M) in THF (2.4 mL) was added dropwise over 15 min. The resulting mixture was refluxed for 24h. The reaction was then quenched by the addition of water (0.2 mL), and solvent was removed under reduced pressure. The residue was taken up in CH_2Cl_2 and washed with water (5 mL) and brine (5 mL). The organic layer was dried over anhydrous $MgSO_4$(s) and filtered, and solvent was removed under reduced pressure. The residue was purified by flash chromatography (silica gel, 20% EtOAc in CH_2Cl_2). Phosphine oxide **17** (0.12 g) was isolated as a white solid in 52% yield. ^{1}H NMR spectrum of **17** was identical to that reported previously.[56]

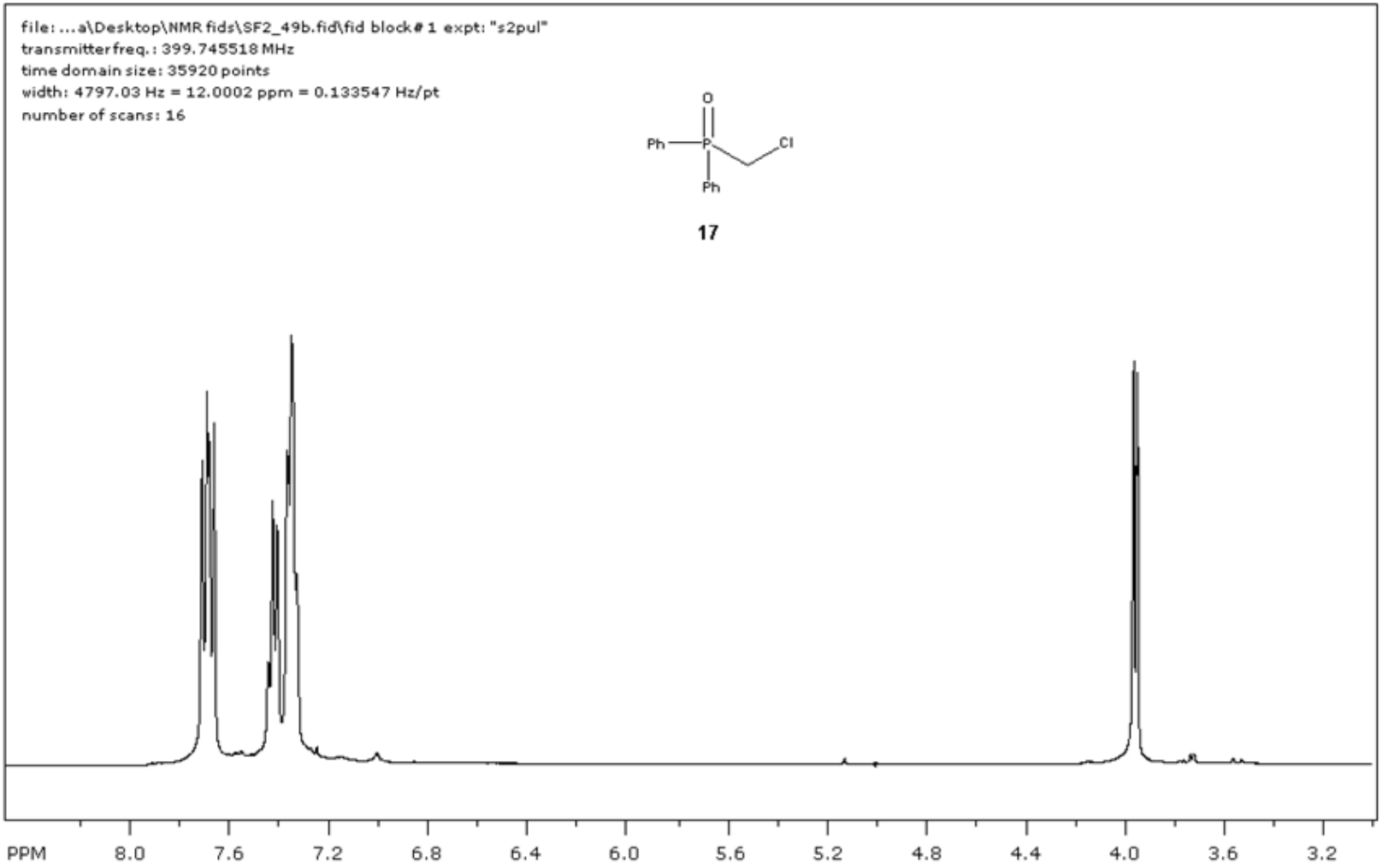

Figure 26. NMR spectrum for **17**

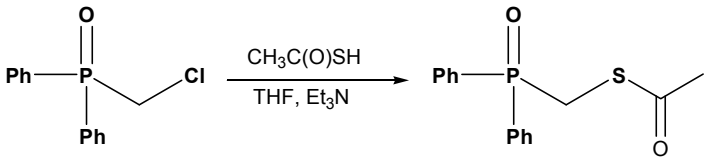

17 **18**

Thiophosphine Oxide (18).[56] Phosphine oxide **17** (40.6 mg, 0.16 mmol) was dissolved in THF (0.96 L). Thioacetic acid (0.07 mL, 1.03 mmol) was added, and the resulting solution was cooled in an ice bath. Argon (g) was bubbled through the reaction mixture for 1h. Diisopropylethyl amine (0.177 mL, 1.07 mmol) was added dropwise, and the resulting mixture was heated at reflux for 24h. Another aliquot of thioacetic acid (0.07 mL, 1.05 mmol) was then added, followed by triethyl amine (0.15 mL, 1.04 mmol). The reaction mixture was heated at reflux for another 24h, after which solvent was removed under reduced pressure. The resulting black oil was dissolved in CH_2Cl_2 (1 mL), and this solution was washed with 2 N HCl (0.3 mL), saturated sodium bicarbonate solution (0.3 mL), and brine (0.3 mL). The organic layer was dried over anhydrous $MgSO_4$(s) and filtered. Activated charcoal was added to this solution, which was then heated at reflux for 30 min. The activated charcoal was removed by filtration, solvent was removed under reduced pressure, and the residue was purified by flash chromatography (silica gel, 70% ethyl acetate in hexane). Thioacetate **18** (22 mg, 48% yield) was isolated as orange oil. ^{1}H NMR spectrum of **17** was identical to that reported previously.[56]

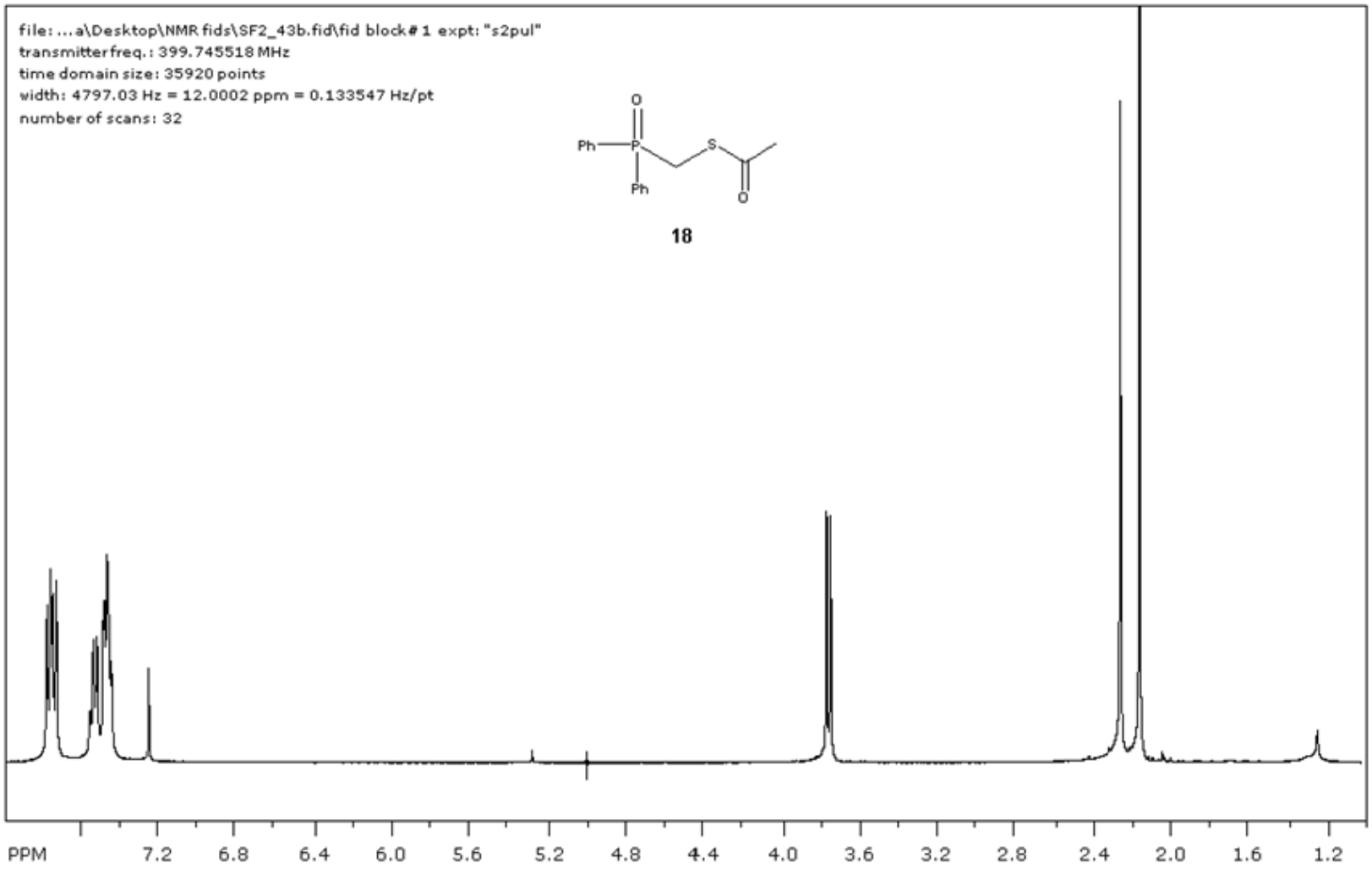

Figure 27. NMR spectrum for **18**

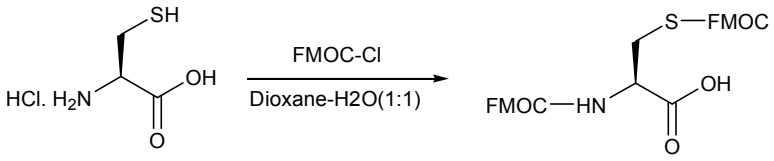

A **22**

2-(9H-fluoren-9-ylmethoxycarbonylamino)-3-(9H-fluoren-9- ylmethoxy carbonyl sulfanyl)-propionic acid; Fmoc-Cys (Fmoc)-OH (22).[55] To a 0°C solution of HCl-Cysteine-OH-H_2O, **A** (351.7 mg, 2.0 mmol) in 20 mL of 50% aqueous dioxane, fmocCl (1.1976 g, 4.6 mmol) was added, and adjusted to pH 7 by addition of 2 N NaOH. Continuous adjustment to pH 7 with 2 N NaOH was done for 5h, at which point the reaction was concentrated *in vacuo* to remove dioxane. Acidification to pH 2 with 1 N HCl was followed by extraction with CH_2Cl_2 (3 x 100 mL). The organic layers were combined, dried over $MgSO_4$, filtered, concentrated *in vacuo*, and purified by flash column chromatography (SiO_2, 94/5/1) CH_2Cl_2/MeOH/AcOH, to give a white foam. The product was recrystallized from EtOAc/hexanes to give 814.0 mg (72% yield) of product as a white solid. ^{1}H NMR spectrum of **22** was identical to that reported previously.[55]

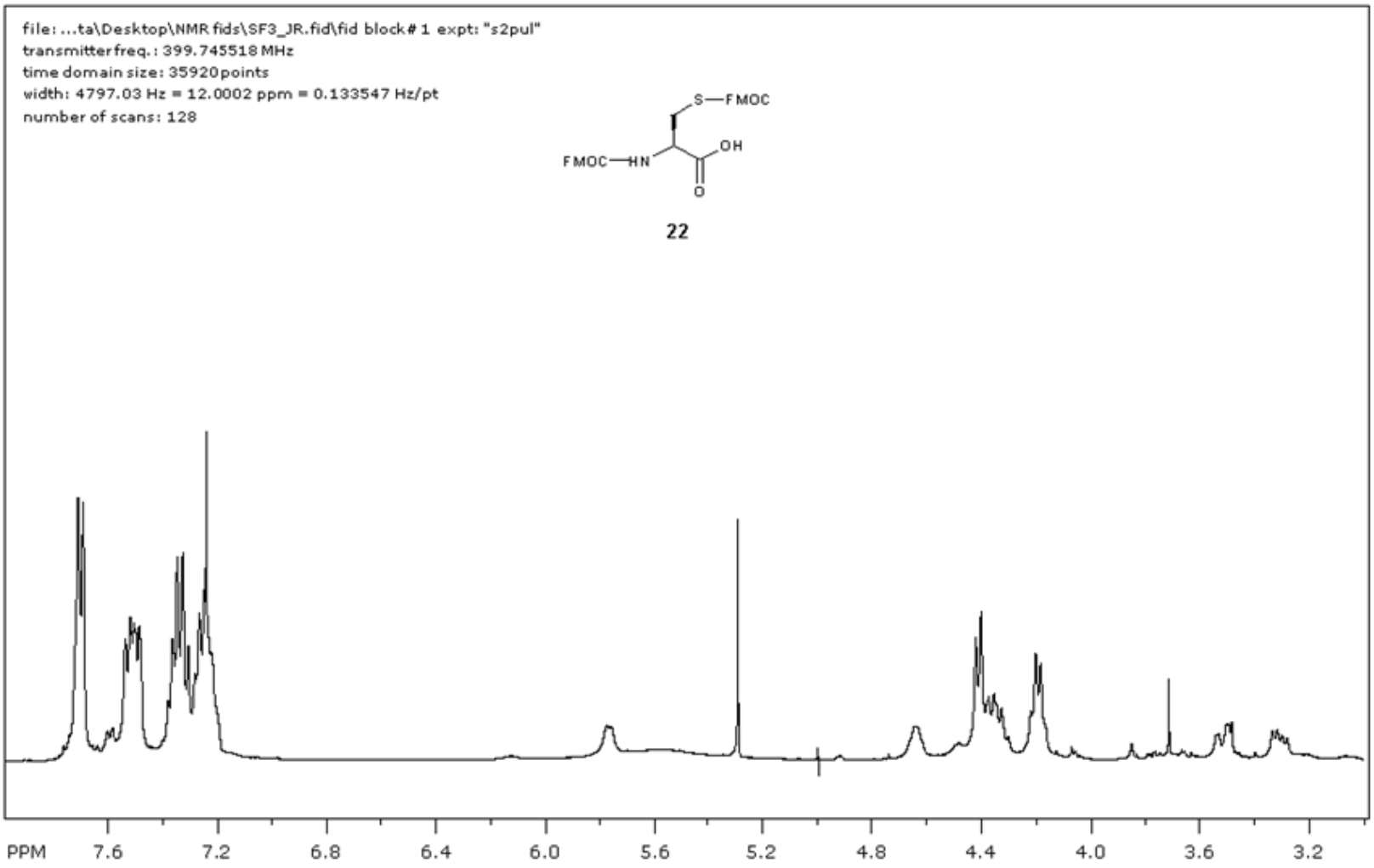

Figure 28. NMR spectrum for **22**

REFERENCES

(1) Guo, Z. W.; Bishop, L. *Eur. J. Org. Chem.* **2004**, *1*, 3585-3596.
(2) VarelaNieto, I.; Leon, Y.; Caro, H. N. *Comp. Biochem. Physiol.* **1996**, *115*, 223-241.
(3) Ferguson, M. J.; Homans, S. W.; Dwek, A.; Rademacher, T. W. *Science* **1988**, *239*, 753-759.
(4) Nosjean, O.; Briolay, A.; Roux, B. *Biochim. Biophys. Acta* **1997**, *1331*, 153-186.
(5) Low, M.; Hoessli, D.C.; and Ilangumaran S. GPI-anchored molecules-an overview, in GPI-anchored membrane proteins and carbohydrates; *Landes Company*, Austin, TX. **1999**, *1*, 1-14.
(6) Paulick, M.; Bertozzi, C. *Biochemistry* **2008**, *47*, 6991-7000.
(7) Jones, D. R.; Varela-Nieto, *Mol. Med.* **1999**, *5*, 505-514.
(8) Larner, J.; Price, J. D.; Heimark, D.; Smith, L.; Rule, G.; Piccariello, T.; Fonteles, M. C.; Pontes, C.; Vale, D.; Huang, L. *J. Med. Chem.* **2003**, *46*, 3283-3291.
(9) Leon, Y.; Varela-Nieto, I. *Lipases and Phospholipases in Drug Discovery*; Muller, G.; Petry, S.; Wiley: New-York **2004**, *1*,101-119.
(10) Saltiel, A. R.; Cuatrecasas, P. *Proc. Natl. Acad. Sci. U.S.A.* **1986**, *83*, 5793-5797.
(11) Mato, J. M.; Kelly, K. L.; Abler, A.; Jarett, L. *J. Biol. Chem.* **1987**, *262*, 2131-2137.
(12) Misek, D. E.; Saltiel, A. R. *J. Biol. Chem.* **1992**, *267*, 16266-16273.
(13) Larner, J. *J. Cyclic Nucl. Res.* **1982**, *8*, 289-296.
(14) Stolar, M; Hoogwerf, B; Boyle, P; Gorshow, S.; Wales, D. *J. Manag. Care Pharm.* **2008**, *14*, 1-19.
(15) Toft-Nielsen, M.; Damholt, M.; Madsbad, S.; *J. Clin. Endocrin. Metab.* **2001**, *86*, 3717-3723.
(16) Virally, M.; Blickle, J.F.; Girard, J.; Halimi, S.; Simon, D.; Guillausseau, P. *Diabetes Metab.* **2007**, *33*, 231-244.
(17) Bjornholm, M.; Zierath, J. *Biochem. Soc. Trans.* **2005**, *33*, 354-357.
(18) Decker, S.; Saltiel, A. *Nat. Med.(New York, ny, U.S.)* **2005**, *11*, 123-124.
(19) Whiteman, E.; Cho, H.; Brinbaum M. *Trends Endocrin. Metab.* **2002**, *13*, 444-451.
(20) Saltiel, A. R.; Kahn, C. R. *Nature* **2001**, *414*, 799-806.
(21) Schinner, S.; Scherbaum, W. A.; Bornstein, S. R.; Barthel, A. *Diabetic Med.* **2005**, *22*, 674-682.
(22) Cohen, A.; Combs, T.; Scherer, P.; Lisanti, M. *Am. J. Physiol. Endocrinol. Metab.* **2003**, *285*, 1151-1160.
(23) Fagerholm, S.; Örtegren, U.; Karlsson, M.; Ruishalme, I.; Strålfors P. *PLoS ONE* **2009**, *4*, 1-10.

(24) Di Guglielmo, M.; Drake, P.; Baass, P.; Authier, F.; Posner, B. I.; Bergeron, J. *Mol. Cell. Biochem.* **1998**, *182,* 59-63.
(25) Elchebly, M.; Payette, P.; Michaliszyn, E.; Cromlish, W.; Collins, S.; Loy, A.; Normandin, D.; Cheng, A.; Himms-Hagen, J.; Chan, C.C. *Science* **1999**, *283*, 1544-1548.
(26) De Fea, K.; Roth, R. *Biochemistry* **1997**, *36*, 12939-12947.
(27) Aguirre, V.; Uchida, T.; Yenush, L.; Davis, R.; White, M. *J. Biol. Chem.* **2000**, *275*, 9047-9054.
(28) Yu,C.; Chen, Y.; Cline, G.; Zhnag, D.; Zong, H.; Wang, Y.; Bergeron, R.; Kim, J.; Cushman, S.; Cooney, G.; *J. Biol. Chem.* **2002**, *277*, 50230-50236.
(29) Hauner, H. *Diabetes Metab. Res.* **2002**, *2*, 135-142.
(30) Davidson, J. *J. Am. Pharm. Assoc.* **2009**,*1*, 16-29.
(31) Gallwitz, B. *Rev. Diabet. Stud.* **2005**, *2*, 61-69.
(32) Larner, J.; Brautigan, D.; Thorner, M.; *Mol. Med.* **2010**, *16*, 543–551.
(33) Kilgour, E. *Cell. Signal* **1993**, *5*, 97–105.
(34) Jones, D.; Varela-Nieto, I. *Int. J. Biochem. Cell Biol.* **1998**, *30*, 313–326.
(35) Larner, J.; Galasko, G.; Cheng, K.; DePaoliRoach, A.; Huang, L.; Daggy, P.; Kellog, J. *Science* **1979**, *206*, 1408-1410.
(36) Saltiel, A. R. *Endocrinology* **1987**, *120*, 967-972.
(37) Larner, J.; Huang, L. C.; Suzuki, S.; Tang, G.; Zhang, C.; Schwartz, C. F. W.; Romero, G.; Luttrell, L.; Kennington, A. S. *Ann. N.Y. Acad. Sci.* **1989**, *573*, 297-305.
(38) Turner, D. I.; Chakraborty, N.; d'Alarcao, M. *Bioorg. Med. Chem. Lett.* **2005**, *15*, 2023-2025.
(39) Muller, G*. FEBS Lett*. **2002**, *531*, 81-87.
(40) Muller, G.; Hanekop, N.; Kramer, W.; Bandlow, W.; Frick, W. *Arch. Biochem. Biophys.* **2002**, *408*, 17-32.
(41) Goel, M.; Azev, V. N.; d'Alarcao, M. *Future Med. Chem.* **2009**, *1*, 95-118.
(42) Suzuki, S.; Sugawara, K.; Satoh, Y.; Toyota, T. *J. Biol. Chem.* **1991**, *266*, 8115-8121.
(43) Larner, J.; Huang, L. C.; Schwartz, C. F. W.; Oswald, A. S.; Shen, T. Y.; Kinter, M.; Tang, G.; Zeller, K. *Biochem. Biophys. Res. Commun.* **1988**, *151*, 1416-1426.
(44) Plourde, R.; Dalarcao, M.; Saltiel, A. R. *J. Org. Chem.* **1992**, *57*, 2606-2610.
(45) Frick, W.; Bauer, A.; Bauer, J.; Wied, S.; Muller, G. *Biochemistry* **1998**, *37*, 13421-13436.
(46) Chakraborty, N.; d'Alarcao, M. *Bioorg. Med. Chem.* **2005**, *13*, 6732-6741.
(47) Azev, V. N. Synthesis of 1,2-diamino-1,2-dideoxymyoinositol and its derivatives and synthesis of palmitoylated inositol glycans. Ph.D, Tufts

University, Medford, MA, **2007**.
(48) Goel, M. Synthesis of a potentially insulin-mimetic, lipid-linked inositol glycan. M.S. San Jose State University, San Jose, CA, **2010**.
(49) Robinson, P.; Millrain, M.; Antoniou, J.; Simpson, E.; Mellor, A. *Nature* **1989**, *342*, 85-87.
(50) Saxon, E.; Armstrong, J.; Bertozzi, C. *Org. Lett*. **2000**, *14*, 2141-2143.
(51) Soellner, B.; Nilsson L.; Raines R. *J. Am. Chem. Soc.* **2006**, *128,* 8820-8828.
(52) Mallik, R.; Wa, C.; Hage, D. *Anal. Chem*. **2007**, *79*, 1411–1424.
(53) Jaworek, C. H.; Iacobucci, S.; Calias, P.; d'Alarcao, M. *Carbohydr. Res.* **2001**, *331*, 375-391.
(54) Kohn, M.; Breinbauer, R. *Angew. Chem. Int. Ed.* **2004**, *43*, 3106-3116.
(55) West, W.C.; Estiarte, M.A.; Rich, H.D. *Org. Lett.* **2001**, *3*, 1205-1208.
(56) Nilsson, B.; Kiessline, L.; Raines, R. *Org. Lett*. **2001**, *3*, 9-12.
(57) Zapata A., Leon Y., Mato, M., Varela-Nieto, I., Penades, S., Martin-Lomas, M. *Carbohydr. Res*. **1994**, *264*, 21-31.
(58) Tsuda, Y.; Nunozawa, T.; Yoshimoto, Y. *Chem. Pharma. Bull*. **1980**, *28*, 3223-3231.
(59) Tejima, S.; Ness, R.; Kaufman, R.; Fletcher H. *Carbohydr. Res*. **1968**, *7*, 485-490.
(60) Kireey, A.; Nadein, O.N.; Agustin, V.J.; Bush, N.E.; Evidente, A.; Manpadi, M.; Ogasaware, M.; Rastogi, S.K.; Rogelj, S.; Shors, S.T.; Kornienko, A. *J. Org. Chem.* **2006**, *71*, 5694-5707.
(61) Mancuso, A.J.; Huang, S.L.; Swern, D. *J. Org. Chem.* **1978**, *43*, 2480-2482.
(62) Kornienko, A. Practical enatiospecific synthesis of differentially protected cyclitols and partial syntheses of a non-hydrolyzable phosphooligosaccharide analog related to insulin signal transduction. Ph. D, Tufts University, Medford, MA, **1999**.
(63) Hansen, F.; Bundgroud E.; Madsen, R. *J. Org. Chem.* **2005**, *70*, 10139-10142.
(64) Tron, G.; Pirali, T.; Billington, R.; Canonico P.; Sorba, G.; Genazzani, A. *Med. Res. Rev*. **2008**, *28*, 278-308.
(65) Smrt, J.; Catlin, J. *Tetrahedron Lett.* **1970**, *11*, 5081-5082.
(66) Hunter, R.; Kaschula,C.H.; Parker, M.; Caira, M.R.; Richards, P.; Travis, S.; Taute, F.; Qwebani. T. *Bioorg. Med. Chem. Lett*. **2008**, *18*, 5277-5279.
(67) Diaz, L; Bujos, J.; Casas, J.; Llebaria, L.; Delgado, A. *J. Med. Chem*. **2010**, *53*, 5248-5255.
(68) Luchetti, G.; Ding, K.; d'Alarcao, M.; Kornieko, A. *Synthesis*. **2008**, *19*, 3142-3147.
(69) Werner, L.; Hudlicky, J.R.; Wernerova, M.; Hudlicky, T. *Tetrahedron* **2010**, *66*, 3761-3769.

(70) Azev, A.N.; d'Alarcao, M. *J. Org. Chem.* **2004**, *69*, 4839-4842.
(71) Carruthers, W. *Some modern methods of organic synthesis.* Cambridge University Press, **1986**, *3,* 221-222.
(72) Gonzalez-Bulnes, P.; Casas, J.; Delgado, A.; Llebaria, A. *Carbohydr. Res*. **2007**, *342*, 1947-1952.
(73) Podeschwa, M.; Plettenburg, O.; Altenbach, H. *Org. Biomol. Chem.* **2003**, *1*, 1919-1929.